



Detailed engineering geological assessment of a shotcrete lined pressure tunnel in the Himalayan rock mass conditions: a case study from Nepal

Chhatra Bahadur Basnet¹ · Krishna Kanta Panthi¹

Received: 12 August 2018 / Accepted: 12 May 2019 / Published online: 8 June 2019
© The Author(s) 2019

Abstract

The complex topography, geology, and tectonic environment prevailing in the Himalaya are the main challenges while applying the unlined or shotcrete lined pressure tunnel concept for hydropower projects. In addition, rock masses in the Himalayan region are influenced by faulting, folding, schistosity, and jointing to a varying degree representing geological complexity. Similarly, frequent occurrence of large scale earthquakes changes in situ stress dynamics. In spite of these challenges, an unlined/shotcrete lined pressure tunnel is being constructed at the headrace tunnel system of Upper Tamakoshi Hydroelectric Project (UTHP) in the Nepal Himalaya. This article studies the unlined or shotcrete lined pressure tunnel in terms of the topographical conditions, in situ stress state, and overall rock engineering aspects. First, the pressure tunnel alignment is assessed using the Norwegian confinement criteria. Second, the minimum principal stress state is assessed using numerical simulation by validating measured in situ stress conditions. Finally, a comprehensive assessment on the rock engineering aspects of the headrace tunnel is carried out. It has been found that if there exist good quality rock mass with tight joints, it is possible to apply the unlined/shotcrete lined pressure tunnel system in the Himalaya provided that the stress requirement is fulfilled. It was also found that the Norwegian confinement criteria are too optimistic for direct use in the design of high pressure headrace tunnel alignment. The detailed rock engineering assessment and stress state analysis indicated that there are some critical locations along the Upper Tamakoshi headrace tunnel alignment. This is specially the case for an about 700 m downstream stretch of the headrace tunnel from where there is a risk of hydraulic jacking, which may possibly lead to excessive water leakage during power plant operation.

Keywords Himalayan geology and tectonics · Topography · Unlined/shotcrete lined pressure tunnel · Confinement criteria · Rock engineering assessment · In situ stress state · 3D model

Introduction

In an unlined pressure tunnel/shaft of a hydropower scheme, water gives pressure to the rock mass around the tunnel periphery equal to the pressure given by the vertical water column measured from ‘head water level’ (HWL) to the point of consideration. This pressure is further termed water pressure

(P_w) and is illustrated in Fig. 1. It is obvious to argue that the water pressure should be resisted by some counter pressure to avoid failure of rock mass around the tunnel. Based on this hypothesis, several design concepts came into practice in the history of unlined pressure tunnels (Palmstrom and Broch 2017). However, a common requirement for all criteria is that the rock mass around the tunnel should be safe against hydraulic jacking (Basnet and Panthi 2018b). Two fundamental aspects were considered while defining different design criteria for unlined tunnels, i.e., the topography (overburden) and the in situ stress state. It is hence practical to mention a brief history of the development of design criteria for unlined tunnels to better understand the concept and its applicability to the variety of topographical and stress conditions.

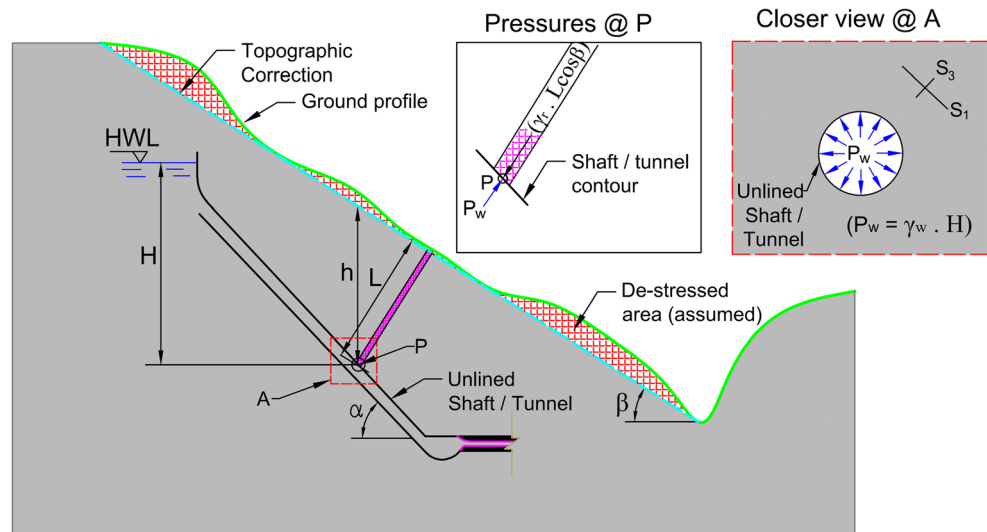
Early in the 1920s, Vogt (1922) highlighted that requirement for the application of an unlined pressure tunnel/shaft is that there should be no leakage from such tunnels and shafts

✉ Chhatra Bahadur Basnet
chhatra.basnet@ntnu.no

Krishna Kanta Panthi
krishna.panthi@ntnu.no

¹ Department of Geoscience and Petroleum, Norwegian University of Science and Technology, Sem Saelands Vei 1, 7491 Trondheim, Norway

Fig. 1 Different parameters used in different design criteria for unlined shaft/tunnel (Note: S_1 is major principal stress, S_3 is minimum principal stress, and HWL is head water level)



(Broch 1982). Talobre (1954) (in Rancourt 2010) on the other hand proposed that the topographic level above the tunnel must be above the head water level (reference to HWL in Fig. 1). Later in 1962, Terzaghi (1962) proposed a relationship, which indicates that the weight of vertical rock cover should be greater than the water pressure in the tunnel and shaft. Snowy Mountain Hydroelectric Authorities in Australia expanded the Terzaghi's relationship, including slope topography as well the horizontal rock cover distance, which should be twice the vertical cover (Dann et al. 1964). In Norway, before 1968 the so called 'rule of thumb' was used in the design of unlined pressure shaft and tunnel. According to the Norwegian rule of thumb, the vertical rock cover from the tunnel should be greater than the hydrostatic head (H) multiplied by a factor ranging from 0.6 to 1.0 depending on the valley slope angle (Broch 1982). However, after a failure occurred at the Byrte project in 1968, the rule of thumb was modified with a concept that the ground pressure given by vertical rock cover should be greater than the water pressure so that hydraulic jacking is avoided (Selmer-Olsen 1969). Mathematically, the criterion is expressed by Eq. 1 and the corresponding factor of safety (FoS_1) is given by Eq. 2.

$$h > \frac{P_w}{\gamma_r \times \cos\alpha} \quad (1)$$

$$FoS_1 = h \times \left(\frac{\gamma_r \times \cos\alpha}{P_w} \right) \quad (2)$$

Where h is the vertical rock cover above tunnel, H is the hydrostatic head acting in the tunnel, γ_w is the specific unit weight of water, γ_r is the specific unit weight of the rock, and α is the inclination of shaft/tunnel with respect to horizontal plane (Fig. 1). The criterion represented by Eq. 1 was governed by the principle that the vertical pressure from rock mass above the tunnel is enough to counteract the water

pressure acting on it. This condition is applicable at relatively flat ground where the horizontal stress is significantly contributed by the tectonic stress. However, the ground is not always flat; rather it is characterized by typical slope topography in the areas where hydropower plants are located. This condition imposed more challenges in reality when a failure occurred in an unlined pressure tunnel at Askara project in 1970 where the tunnel was initially designed by using the criteria defined by Eq. 1. This failure asserted the Norwegian design engineers to modify the criterion. The criterion was then modified by incorporating the slope topography to calculate the resisting ground pressure against water pressure. The criterion is mathematically expressed by Eq. 3 and the corresponding factor of safety (FoS_2) is given by Eq. 4.

$$L \cos\beta > \frac{P_w}{\gamma_r} \quad (3)$$

$$FoS_2 = L \cos\beta \times \left(\frac{\gamma_r}{P_w} \right) \quad (4)$$

Where L is shortest distance from the ground profile to the tunnel location and β represents the angle of valley side slope with respect to horizontal plane. Both the criteria represented by Eqs. 1 and 3 are commonly known as the Norwegian criteria for confinement (Selmer-Olsen 1969; Bergh-Christensen and Dannevig 1971; Broch 1982; Panthi 2014; Palmstrom and Broch 2017). It is highlighted here that the Norwegian confinement criteria have been accepted and are being used in the design of unlined or shotcrete lined pressure tunnels and shafts around the world. In addition to these criteria, a concept came in 1984 that a topographic correction in an undulated ground surface is required to refine the geometrical parameters as shown in Fig. 1 (Broch 1984). The concept was based on the principal that the rock mass outside of the correction line is supposed to have negligible

contribution to the confinement (de-stressed area indicated in Fig. 1). It is further highlighted that the criterion defined by Eq. 3 was not adequate in some Norwegian projects and one more criterion was evolved with the concept of minimum principal stress after the 1970s. The criterion is that the in situ minimum principal stress (S_3) should always be greater than the water pressure inside the tunnel in order to ensure the safety against hydraulic jacking (Selmer-Olsen 1974; Broch 1982; Basnet and Panthi 2018b). The criterion is the state-of-the-art in the design of unlined or shotcrete lined pressure tunnel and shaft and is represented by Eq. 5. The corresponding factor of safety (FoS_3) is given by Eq. 6.

$$S_3 > P_w \quad (5)$$

$$FoS_3 = \frac{S_3}{P_w} \quad (6)$$

Furthermore, Basnet and Panthi (2018a) proposed both favorable and unfavorable ground conditions for the applicability of the confinement criteria based on the study carried out for Norwegian failure and successful unlined pressure shaft and pressure tunnel cases. In the unfavorable ground conditions, they concluded that the stress state of the area needs to be estimated in order to explore the safe location of unlined tunnel. This is of paramount importance in the case of steep slope topography where the stress generated by gravity and/or generated because of tectonics is attenuated by the slopes in different directions in a complex topography. Besides, the presence of faults, weakness zones, and unfavorable jointing in the rock mass at the area of unlined pressure tunnel imposes more challenges.

Outside of Norway, a shotcrete lined pressure tunnel is being implemented at the Upper Tamakoshi Hydropower Project (UTHP) in Nepal. As the name suggests, the pressure tunnel is provided with a thin layer of shotcrete lining (5 to 15 cm thick) as final rock support. The thin layer of shotcrete liner (less than 15 cm) in general has porosity exceeding 20%, indicating shotcrete as a highly permeable material (Holter et al. 2014). Hence, the shotcrete lining should be considered as a permeable support liner unless the shotcrete lining is designed with a water proof membrane. The fact is that the water proof membrane is not suitable for water tunnels due to the buildup of pressure between the shotcrete liner and the rock mass, which may lead to the failure on the shotcrete liner. In addition, in a water tunnel where shotcrete is applied as support, about one-meter long drain holes are drilled along the periphery of the tunnel to reduce the risk of water pressure buildup between the shotcrete liner and the rock wall. The drain holes function as medium to make flowing water in direct contact with the rock mass. Therefore, almost equal water pressure will act on the rock mass as that on the shotcrete lining (Brekke and Ripley 1987). As a matter of fact, the shotcrete lined tunnel at UTHP is analyzed with the same

criteria as that for an unlined tunnel. The topography and rock mass at UTHP area are studied in detail in order to explore whether the area satisfies the conditions needed for the implementation of a shotcrete lined high pressure tunnel or not. Reasons for lack of success in the originally planned headrace tunnel alignment with 420 m water head are evaluated in great detail. The design of the new alignment is comprehensively reviewed. Both old and new alignments are analyzed in detail using the Norwegian confinement criteria, rock engineering aspects, and in situ stress state.

Brief on upper Tamakoshi project

The Upper Tamakoshi Hydroelectric Project (UTHP) is located at about 90 km northeast from Kathmandu, Nepal (Fig. 2a). The project has an installed capacity of 456 MW and exploits the design discharge of 66 m³/s and 822 m gross hydrostatic water head. The project consists of a low head diversion dam, settling basins, headrace tunnel, vertical shafts, underground powerhouse, tailrace tunnel, and access tunnel (Fig. 2b and c). Geologically, the project is located in the Higher Himalayan Tectonic Formation of eastern Nepal Himalaya (Fig. 2a). Rock mass in this formation is mainly characterized by Precambrian high grade metamorphic rocks, such as gneiss, quartzite, marbles, magmatite, and granitic gneiss having the quality of rock mass comparable to the Scandinavian hard rock mass ('hx' in Fig. 2a). In particular, the rock type at the project area is characterized by schistose gneiss having three distinct joints sets plus random joints. The project geology is explained in detail by Panthi and Basnet (2017).

From the pre-feasibility study in 2001 until the construction in 2014, there have been several changes to the pressurized headrace tunnel alignment of the UTHP, which was discussed in detail by Panthi and Basnet (2017). In 2008, the unlined/shotcrete lined pressure tunnel was proposed from the inlet portal to the top of the lower penstock shaft (steel lined), which is shown as 'OLD HRT' in Fig. 2b and c. The OLD HRT was planned to have a maximum static water head of about 420 m (4.2 MPa) at the downstream end of the unlined/shotcrete lined headrace tunnel. Later in 2013, the headrace tunnel was shifted up and the downstream segment of the headrace tunnel was further pushed toward the hill side shown as 'NEW HRT' in Fig. 2b and c. In this final alternative of the headrace tunnel alignment, the maximum water head is reduced to about 115 m (1.15 MPa) where the tunnel ends at the top of the upper vertical penstock shaft (steel lined). The magnitude of minimum principal stresses measured at different locations at different times in the history played a decisive role in the modification of the tunnel alignment. The overall stress measurement campaign therefore became very crucial for the design of the unlined/shotcrete lined pressure tunnel at the UTHP.

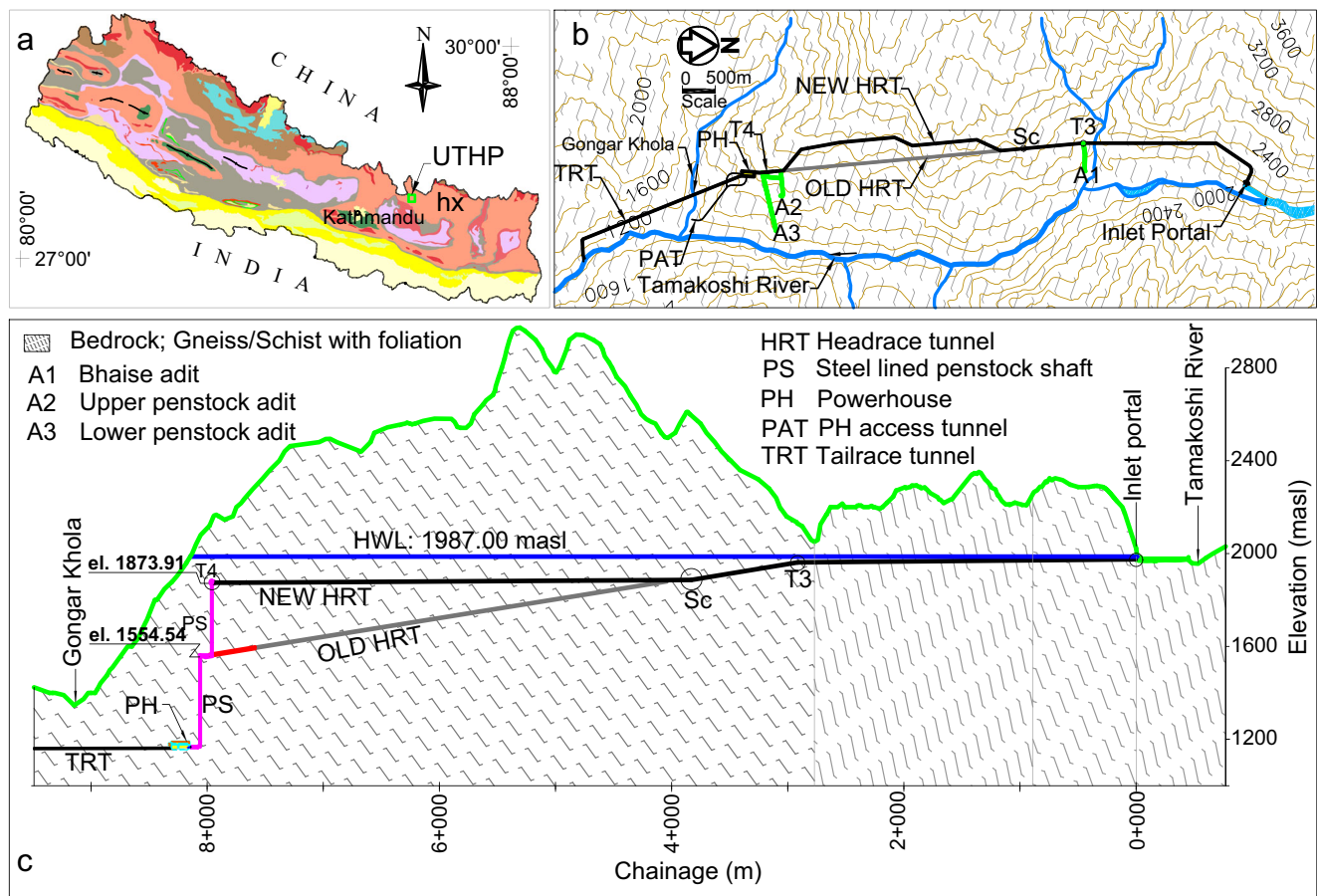


Fig. 2 a Location of the UTHP in geological map of Nepal; b Layout plan of two different alternatives of headrace tunnel of the UTHP; c Profile along the alignment of the UTHP (Note: ‘masl’ is meters above sea level)

In situ stress measurement

At the UTHP, both 3D overcoring and hydraulic fracturing/hydraulic jacking techniques were used to measure the in situ stress state at different locations as shown in Fig. 3. The measurements were carried out at three different elevation levels of the topography at different phases of design and construction.

3D Overcoring (OC)

In 2008, three dimensional stresses were measured at locations TT1, TT2, and TT3 in the test tunnel (TT) by using the 3D overcoring technique (SINTEF 2008). The details of the test location plan is shown in Fig. 4. The figure also shows location details of the measurement points and the topographic condition. Three measurements in the bore hole were performed at locations TT1 and TT2 at depths 6 m, 6.5 m, and 7 m from tunnel face, respectively. SINTEF (2008) highlighted that the stress measurement at TT3 was disturbed owing to water ingress and only one measurement was performed at 8 m depth. The standard overcoring

technique as is being practiced around the world was used in the stress measurement.

The computer program called Determination of In situ Stress by Overcoring (DISO) developed by SINTEF (Lu 2006) was used to calculate the magnitude and the orientation of principal stresses from the strain readings and use of elastic parameters. The parameters, such as density, Young’s modulus of elasticity, and Poisson’s ratio were determined by laboratory testing. The DISO program is a statistical calculation tool that analyses stress parameters giving mean values of principal stresses with standard deviations and orientation of corresponding stresses. The computed stress magnitude and orientations are presented in Table 1. In the table, a very low magnitude of S_3 at TT2 compared to the other two locations is noticed. The unexpectedly low measured minimum principal stress at location TT2 was inferred to be attributed to the presence of nearby fracture zones.

The overcoring stress results indicated that the ‘OLD HRT’ alignment proposed in 2008 as unlined/shotcrete lined tunnel was safe for implementation, which was originally designed using the Norwegian confinement criteria. The assumption on this pre-construction phase design was that the minimum principal stress would most likely be sufficient to safeguard the

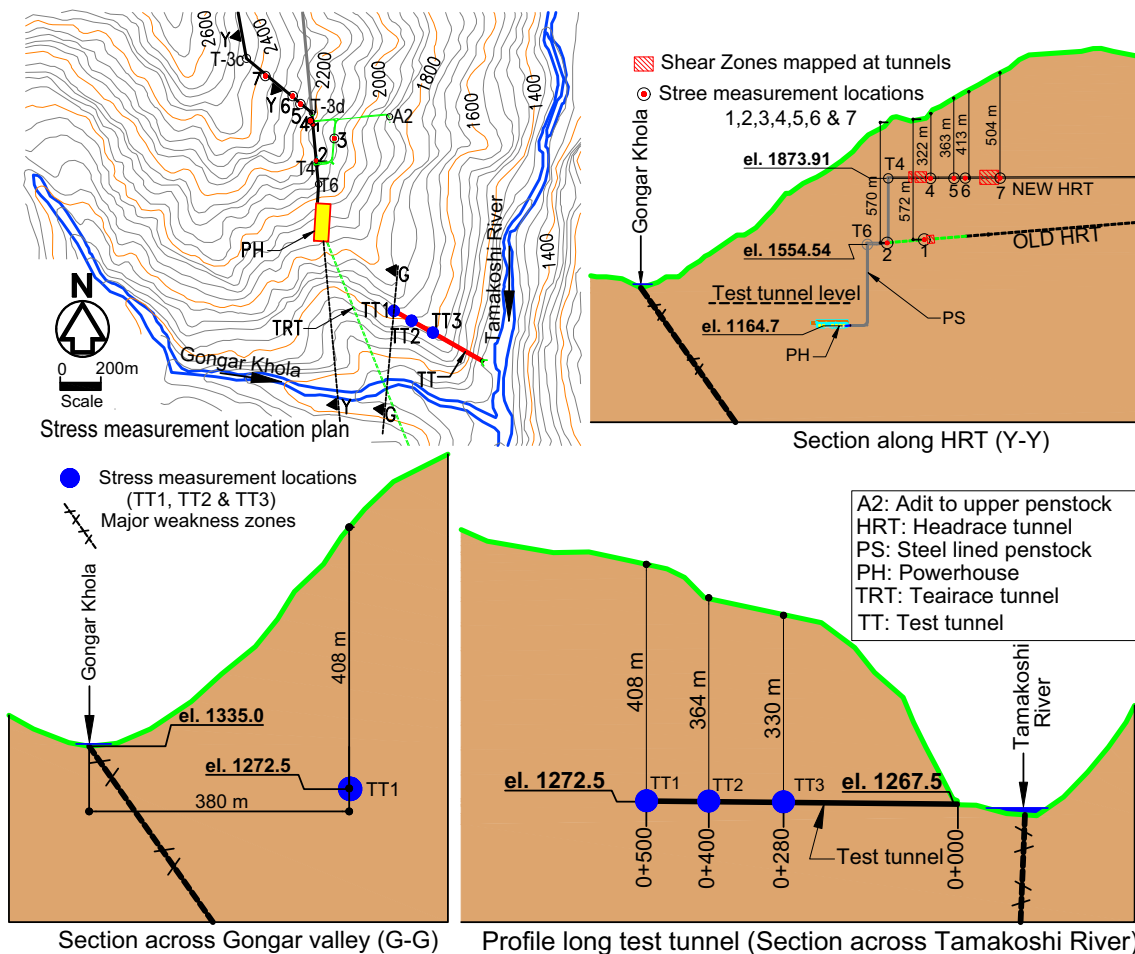


Fig. 3 Stress measurement locations TT1, TT2, TT3, 1, 2, 3, 4, 5, 6, & 7 (Note: all dimensions are in meter)

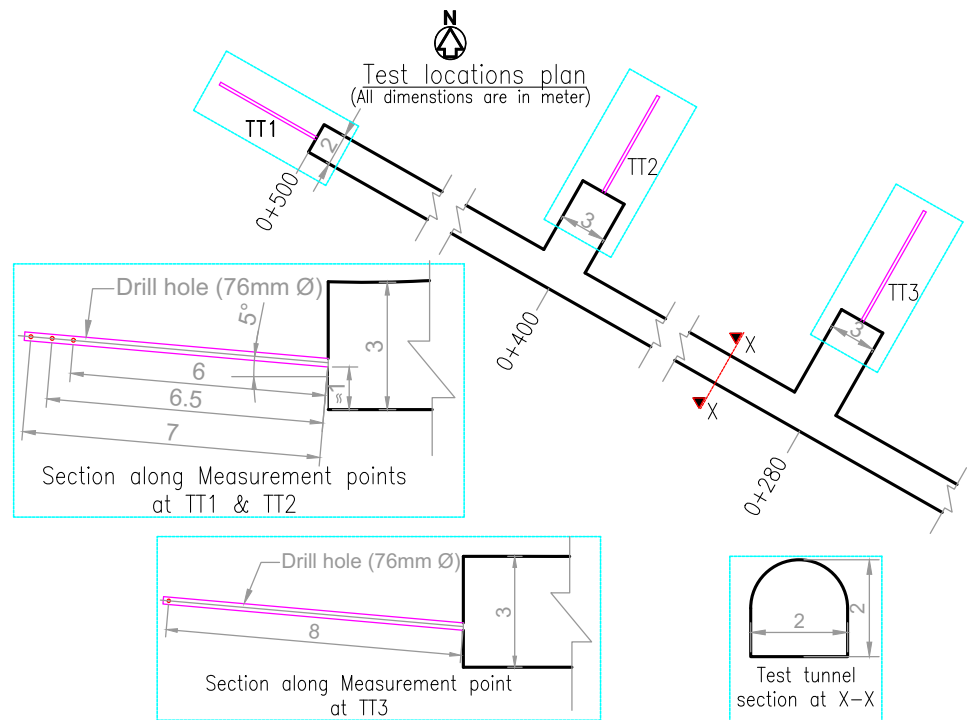
rock mass from hydraulic jacking due to the water head of about 420 m. Still, it was recommended that the magnitude of minimum principal stress is measured at the downstream end of the headrace tunnel during excavation.

Hydraulic fracturing (HF)/hydraulic jacking (HJ) tests

Following the recommendation during design, the magnitude of minimum principal stress was measured at locations 1 and 2 along the excavated headrace tunnel at the downstream end by using the hydraulic fracturing technique (Figs. 3 and 5). The measurement procedure followed was similar to that suggested by the International Society for Rock Mechanics (Haimson and Cornet 2003). However, an exception in this test was that the fracture orientation was not determined since the purpose of the test was just to measure the magnitude of minimum principal stress. The measurement details and test results are explained in detail by SINTEF (2013). The test equipment was placed at a desired borehole depth and two packers are inflated with water, closing a borehole section

of about 1.0 m. At each test section, the initial fracture was induced in the isolated borehole in the in situ rock mass by pumping water. The water pressure required to induce the initial fracture is fracturing pressure ' P_f '. The test was then followed by re-openings of the induced fracture. The pressure required to re-open the fracture is fracture re-opening pressure ' P_r '. The applied water pressure, packer pressure, and water flow rate were continuously logged during the whole test period. The shut-in pressure was identified at a point where the flow was closing in the test section. In each test section in the borehole, at least three test cycles were performed. Finally, the shut-in pressure at each cycle was considered as the magnitude of minimum principal stress at the test location. All three pressures at different measured locations are listed in Table 2. The table also indicates some unsuccessful tests where the water pressure was not able to make a new distinct crack; rather water was lost through permeable pre-existing cracks or joints in the test section or entire borehole depth. Even excluding the unsuccessful tests, the minimum value of minimum principal stresses ($P_{si} = S_3$) at

Fig. 4 Stress measurement details at locations TT1, TT2, and TT3



both locations were found far lower than the pressure from the 420 m water head. It was then concluded that the unlined/shotcrete lined tunnel at the OLD HRT was not safe for a 420 m water head and as a result the ‘NEW HRT’ alignment was proposed.

Two more stress measurement campaign were conducted in 2014 at locations 3, 4, 5, and 6 (MSG 2014) and 2015 at location 7 (MSG 2015). The locations 4, 5, 6, and 7 were along the NEW HRT alignment and location 3 was at the erection tunnel to the top of the upper penstock shaft (Fig. 3). In these campaigns, both hydraulic fracturing and hydraulic jacking techniques were employed. The detail of stress measurement locations, including location and orientation of test holes, diameter and length of test holes, and size of the tunnel, are illustrated in Fig. 5. The tests were conducted in close agreement with the recommendations of the ISRM standard (Haimson and Cornet

2003), with the exception of the determination of the fracture orientation for the same reasons previously discussed. Numerous tests were conducted in each borehole at different measurement locations. The details of the testing procedure are mentioned in MSG (2014 and 2015). Packer pressure, injection pressure, and flow rate were continuously logged during the testing period for each measurement.

In addition to the previously mentioned three pressures, the jacking pressure ‘ P_j ’ as an additional estimation of the minimum principal stress was measured from the step rate tests. In most cases, the shut-in pressure is equal to the jacking pressure. Table 3 gives the summary of tests results consisting of fracturing pressure, re-opening pressure, shut-in pressure, and jacking pressure at each test section of different boreholes at locations 3, 4, 5, 6, and 7. The table also indicates some unsuccessful tests where

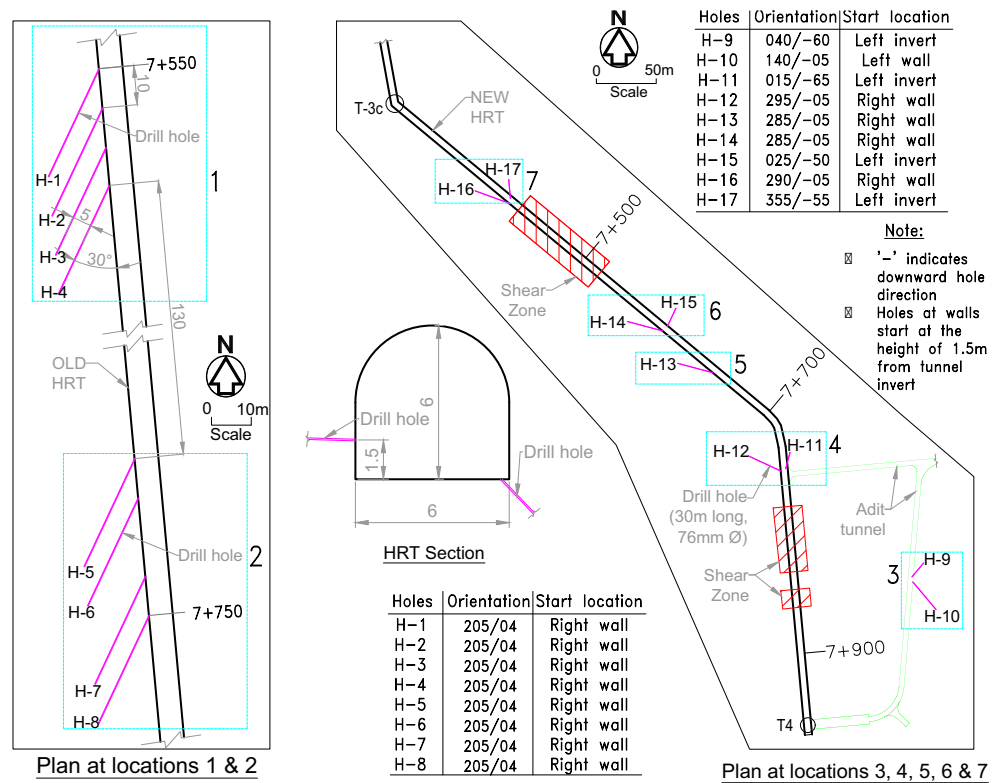
Table 1 Final values of magnitude and orientation of principal stresses at TT1, TT2, and TT3 (Source: SINTEF 2008)

Stresses	TT1			TT2			TT3		
	MPa		Orientation	MPa		Orientation	MPa		Orientation
	Mean	Sd ^b		Mean	Sd		Mean	Sd	
S_1	18.4	2.9	120/28	17.4	2.2	205/30	21.6	3.8	021/10
S_2^a	12.4	4.7	240/42	10.8	1.7	100/23	12.6	2.8	117/27
S_3	7.1	1.8	009/35	1.1	2.7	339/50	6.4	4.8	272/61

^a S_2 is intermediate principal stress

^b Sd is standard deviation

Fig. 5 Location plan details at locations 1, 2, 3, 4, 5, 6, & 7



no pressure was built up because of high permeability. In addition, some tests were also neglected for averaging of minimum principal stress due to unexpectedly high or low values.

Haimson and Cornet (2003) recommended a relationship to estimate the magnitude of maximum principal stress in the case of vertical borehole. Since the bore holes are sub-horizontal or inclined at different locations, the originally recommended relationship is modified keeping in mind that the fracture is induced in the direction perpendicular to minimum principal stress. This brings another fact that the stress parallel to the fracture is obviously the maximum principal stress. Following this hypothesis, the originally recommended relationship is modified and is represented by Eq. 7.

$$S_1 = 3S_3 - P_f + S_t \tag{7}$$

Equation 7 is used to estimate the magnitude of maximum principal stress where S_t is tensile strength of the rock tested in the laboratory by the authors. In summary, Table 5 shows the statistical distribution of magnitude of both maximum and minimum principal stresses at different locations, i.e., 1, 2, 3, 4, 5, 6, and 7. The values given in Table 4 are calculated from Tables 2 and 3.

Review on the OLD headrace tunnel

Unexpectedly, the low value of minimum principal stress measured in locations 1 and 2 did not favor the shotcrete lined pressure tunnel along OLD alignment (Fig. 2). To understand the reasons behind this unfavorable condition, the tunnel is assessed further in detail using the confinement criteria, measured and simulated stress values, and comparing this tunnel with both failure and successful unlined pressure shaft and pressure tunnel cases from Norway.

Analysis with the Norwegian confinement criteria

In the outer reach (downstream end) of the OLD HRT of the Tamakoshi project, the topography has slopes in multiple directions (Fig. 6a). This condition of the topography is very frequent in the Himalayan region. The multiple slopes have different vertical rock covers, lateral rock covers, and valley slope angles for a selected location of an unlined/shotcrete lined pressure tunnel. It is hence necessary to define the representative geometrical parameters required for the confinement criteria in multiple valley slopes. In topography with slopes in different directions, representative values of both vertical rock cover and the term 'Lcosβ' should be minimum of all possible values. Mathematically, both terms can be represented by Eqs. 8 and 9, respectively, where the topographic correction should be applied.

Table 2 Results from test locations 1 and 2 for each hole at different depths (Source: SINTEF 2013)

Location 1							Location 2						
Hole	Hole depth m	P _f MPa	P _r MPa	P _{si} (MPa)			Hole	Hole depth m	P _f MPa	P _r MPa	P _{si} (MPa)		
				1. cycle	2. cycle	3. cycle					1. cycle	2. cycle	3. cycle
H-1	27.5	*	—	—	—	—	H-5	28.6	*	—	—	—	—
	24.5	7.7	4.6	1.8	1.7	1.6		25.6	11.9	9.9	6.7	7.8	8.0
	21.5	*	—	—	—	—		22.6	*	—	—	—	—
	18.5	13.0*	11.0	3.5	3.7	3.7		19.6	10.0	8.8	7.6	7.7	7.4
	15.5	9.2	5.6	3.4	3.3	3.3		16.6	13.5	11.1	7.6	7.7	8.0
	12.5	9.8	5.4	3.4	3.5	3.5		13.6	19.5	9.3	7.8	7.4	7.4
H-2	27.5	11.0	6.4	2.5	2.1	1.9	H-6	28.5	10.5	6.7	5.1	5.0	5.3
	24.5	*	—	—	—	—		25.5	10.1	8.2	5.7	5.8	5.7
	21.5	*	—	—	—	—		22.5	19.1	15.5	8.9	8.7	8.9
	15.5	*	—	—	—	—		19.5	18.7	12.9	9.1	9.1	9.1
H-3	27.0	*	—	—	—	—	H-7	16.5	12.1	10.5	8.9	9.0	9.1
	24.0	*	—	—	—	—		13.5	*	—	—	—	—
	21.0	*	—	—	—	—		27.0	12.5	—	1.8	—	—
	18.0	*	—	—	—	—		25.5	10.1	3.6	2.7	1.9	1.8
	15.0	*	—	—	—	—		24.0	6.4	4.3	2.5	2.3	1.9
	12.0	*	—	—	—	—		18.0	8.4	5.6	3.1	4.0	4.1
H-4	24.0	9.9	7.2	4.9	4.8	4.8	H-8	21.0	*	—	—	—	—
	21.0	8.6	7	3.4	3.5	3.5		15.0	9.5	5.3	4.3	4.3	4.6
	18.0	*	—	—	—	—		12.0	10.8	3.7	1.4	1.2	1.5
	15.0	*	—	—	—	—		27.0	*	—	—	—	—
							24.0	11.1	5.7	3.9	3.8	3.8	
							21.0	*	—	—	—	—	
							18.0	10.8	5.1	4.5	4.4	4.4	
							15.0	6.7	4.7	4.4	3.3	3.4	
							12.0	7.2	6.0	3.9	4.0	3.9	

P_f = Fracturing pressure

P_r = Fracture re-opening pressure

P_{si} = Shut-in pressure

*Unsuccessful tests

$$h = \min(h_i)_{i=1}^n \quad (8)$$

$$L \cos \beta = \min(L_i \cos \beta_i)_{i=1}^n \quad (9)$$

In the equations, n is the total number of slopes in different directions. At both locations 1 and 2 of the OLD HRT, corresponding critical values required for Eqs. 1 and 3 are estimated by using Eqs. 8 and 9, respectively. In doing so, the topographic correction is also applied for each side of the slope.

The geometrical parameters are listed in Table 5. The corresponding factor of safeties given by Eqs. 2 and 4 are calculated using the respective input parameters as given in Table 5. For safe operation of an unlined pressure tunnel at normal operating condition of the power plant, the factor of safeties

should be greater than 1.3 (Benson 1989). The table shows that both factors of safeties (FoS₁ and FoS₂) are greater than 1.3. This indicates that the proposed unlined/shotcrete lined pressure tunnel is safe against hydraulic jacking at locations 1 and 2, which are located at the most critical stretches of the OLD HRT alignment.

In situ stress state assessment

The design criterion defined by Eq. 5 is checked at both location 1 and location 2. The minimum principal stresses measured in 2013 are used to calculate the factor of safety (FoS₃) defined by Eq. 6. From statistical distribution of the measured values, it is found that there is only about 18% probability that the FoS₃ is more than one in location

Table 3 Results from test locations 3, 4, 5, 6, and 7 for each hole at different depths (Source: MSG 2014, 2015)

Hole	Hole depth m	P _f MPa	P _r MPa	P _{si} MPa	P _j MPa	Hole	Hole depth m	P _f MPa	P _r MPa	P _{si} MPa	P _j MPa
Location 3						Location 6					
H-9	13.5	–	–	–	4.8*	H-14	7.5	–	6.2	5.1*	4.9*
	21.3	5.8	3.2	2.5	1.6		11.4	19.0	8.3	5.5	6.8
	24.5	9.3	4.9	4.8	1.9		16.1	11.4	2.5	1.65	2.2
	26.9	13.9	7.9	4.3	4.4		19.0	–	4.2	–	5.0
H-10	10.5	–	2.4	2.5	2.0	H-15	21.0	7.5	4.1	3.7	3.4
	18.0	12.2	5.3	5.4	5.2		22.6	–	–	–	3.4
	21.0	15.4	4.6	2.9	3.2		24.7	–	4.7	4.0	4.3
	23.5	13.5	8.4	4.8	5.6		9.5	Unsuccessful test			
	27.0	9.9	6.5	3.5	4.3	12.4	16.1	11.3	8.9*	10.7*	
Location 4						Location 7					
H-11	11.5	–	–	–	7.7*	H-16	7.5	–	13.2	11.9*	13.8*
	13.5	–	4.7	–	5.7		9.5	10.7	4.9	6.8	7.2
	15.1	–	7.0	4.4	6.5		11.5	7.5	4.4	3.2	4.3
H-12	9.0	**				14.5	**				
	11.0					22.5	**				
Location 5						Location 7					
H-13	9.2	7.8	1.4	–	1.2*	24.8	**				
	12.3	–	3.8	3.6	3.7	H-17	11.0	7.5	2.5	2.8	3.2
	17.8	–	–	–	>1.3		13.5	10.7	3.3	3.0	3.6
	23.0	–	7.7	7.2	7.3		17.6	–	2.2	4.0	–
	25.0	**					22.5	12.0	6.7	8.2	7.9
					27.0		–	6.4	9.6	10.0	

P_j = Jacking pressure

**No pressure built up owing to high permeability

*Neglected for averaging of S₃**Table 4** Summary of test results by hydraulic fracturing at locations 1, 2, 3, 4, 5, 6, & 7

Location	S ₃ (MPa)			S _t (MPa)		S ₁ (MPa)	
	Min	Mean	Sd	Mean	Sd	Mean	Sd
1 ^a	1.6	3.2	1.0	10.0	1.2	10.1	3.2
2 ^a	1.2	5.4	2.5	10.0	1.2	14.2	6.0
3 ^b	1.6	3.7	1.3	10.0	1.2	10.2	3.0
4 ^b	4.4	5.5	1.1	10.0	1.2	–	–
5 ^b	1.3	4.6	2.6	10.0	1.2	–	–
6 ^b	1.7	3.8	1.1	10.0	1.2	9.4	2.8
7 ^c	2.8	5.7	2.7	10.0	1.2	15.3	5.0

^a SINTEF (2013)^b MSG (2014)^c MSG (2015)

1 and about 70% probability in location 2. On the other hand, the mean value of FoS₃ in terms of measured stress is slightly less than one for location 1 and slightly more than one in location 2. It is emphasized here that the minimum value of FoS₃ given by the measured stress is very low in both locations (Fig. 7).

Basnet and Panthi (2018b) used FLAC^{3D} model (ITASCA 2017) to simulate the stress state of the Tamakoshi area covering both locations 1 and 2 of the OLD HRT. Figure 6 shows the simulated values of minimum principal stress along the headrace tunnel profile and along the cross section across location 2. The simulation was carried out considering both without and with the presence of weakness zone. The factor of safety (FoS₃) is calculated by using simulated values of the minimum principal stress for both cases at both locations (Fig. 7). As seen in the figure, FoS₃ is less than 1.3 in both locations and is influenced by the presence of weakness zone, which is

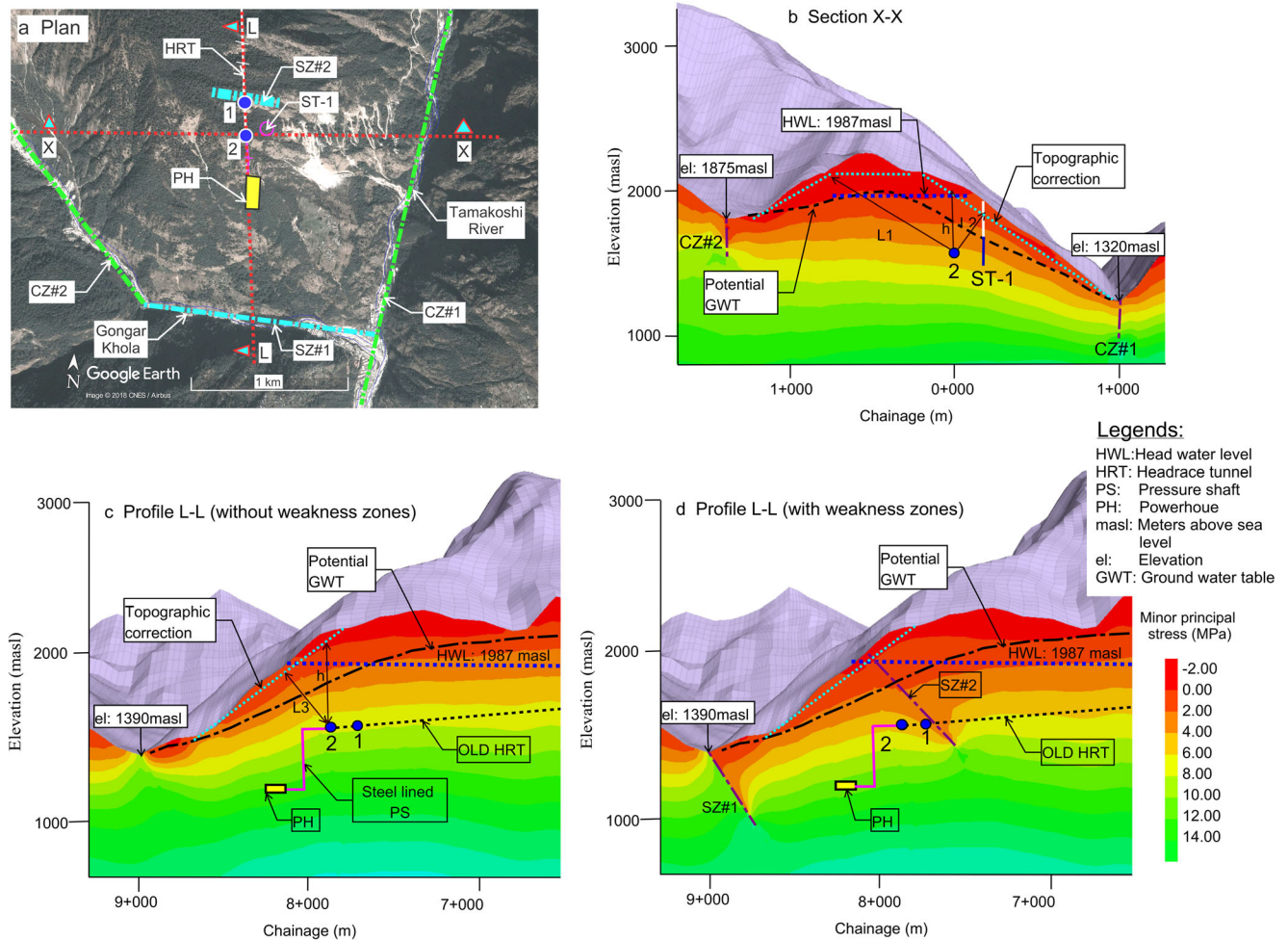


Fig. 6 Plan, section, and profiles at the outer reach of headrace tunnel of Tamakoshi project with minimum principal stress (in color bars), topographic corrections, potential GWT, etc.

mainly due to the de-stressing effect. The analysis result suggests that the minimum principal stress magnitudes are inadequate against hydraulic jacking at both locations. On the other hand, the figure clearly shows that the factors of safety given by the Norwegian confinement criteria are very optimistic compared to FoS_3 .

Comparison with Norwegian failure and successful cases

Basnet and Panthi (2018a) analyzed both failure and successful cases of unlined high pressure shafts and tunnels

of Norway. As an outcome of the analysis, they proposed both favorable and unfavorable ground conditions for the applicability of the Norwegian confinement criteria. Hence, the OLD HRT of the Tamakoshi project is compared with three of the failure cases consisting of an unlined tunnel at the Askara project, unlined shaft at the Byrte project and unlined shaft and tunnel at the Fossmark project; and with one successful unlined tunnel case called Nye Tyin (Table 6).

In Table 6, different important aspects consisting of topography, rock mass and jointing, presence of fault and/or weakness zones, in situ stress state, and hydrogeology are

Table 5 Analysis of OLD HRT of UTHP at locations 1 and 2 using Norwegian confinement criteria

Location	H m	P_w MPa	γ_r MN/ m^3	h m	α Deg.	β Deg.	L m	$L\cos\beta$ m	FoS_1	FoS_2
1	412.2	4.0	0.027	478	0	39	373	289.9	3.19	1.94
2	428.1	4.2	0.027	433	0	40	332	254.3	2.78	1.64

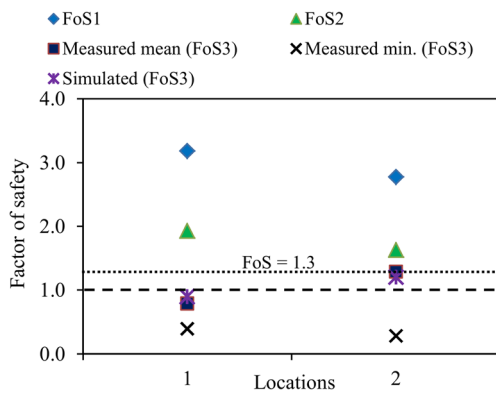


Fig. 7 Factor of safeties at location 1 and location 2

compared between the selected Norwegian cases and the OLD HRT alignment of the UTHP. As one can observe, most of the ground conditions prevailing at the downstream end of the OLD HRT of UTHP do not favor the possibility for an unlined high pressure tunnel (static head of 420 m).

The fact is that the unlined tunnel at the OLD HRT alignment is unfavorable because the minimum principal stress is inadequate to avoid the hydraulic jacking at the most critical studied locations. The low stress values are mainly attributed to the presence of multiple valley topography, weakness zones along major river valleys, and local shear zones crossing the tunnel alignment. The joints in this area are open or filled with loose material due to a decrease in confinement from the Gongar valley side. Open joints and the joints filled with loose material have high conductivity that makes an easier path for water to flow through the joints. In addition, the lower stress values compared to water pressure creates higher probability for hydraulic jacking of the pre-existing joints, which again eases the water flow through the jacked joints. Based on the above analysis and comparison, it is worth saying here that the design modification of OLD HRT was a necessity. Now the concern is whether the NEWLY SHIFTED HRT is safe to be used as an unlined/shotcrete lined tunnel or not. In this regard, thorough assessment and analysis are carried out below by considering all possible aspects, such as topography, rock mass quality, weakness and shear zones, and in situ stress state.

Confinement criteria analysis on the NEW HRT alignment

After the OLD HRT alignment was cancelled, the headrace tunnel of Upper Tamakoshi project was excavated following the new alignment (shown in Figs. 2 and 8 as NEW HRT). The tunnel segment from inlet portal to the point 'T4' is proposed to be an unlined/shotcrete lined tunnel. From inlet portal to the point 'T3', the maximum static water head reaches about 30 m (0.3 MPa) on the tunnel. From 'T3' onward, the tunnel is relatively steeper up to the point 'Sc' where the static water head will reach about 104 m (1.04 MPa). Finally, from

'Sc' onward, the tunnel has gentle slope up to the point T4 (the end of headrace tunnel) where the maximum static water head will reach 115 m (1.15 MPa). Some experience has been gained in the Himalayan region with unlined/shotcrete lined pressure tunnels having less than 40 m water head, and therefore this unlined/shotcrete lined headrace segment from inlet portal to the point of 'T3' should have no significant problem being excluded in areas where rock mass is open jointed or there exists weakness zones. However, the tunnel segment between 'T3' and 'T4' where static water head varies between 30 m and 115 m has a risk of hydraulic jacking and potential water leakage through an unlined/shotcrete lined tunnel. It is therefore important to carry out detailed assessment along this tunnel segment (from 'T3' to 'T4'). The first step of such analysis is to carry out assessment based on the Norwegian confinement criteria for unlined tunnel (i.e., Eqs. 1 and 3) at selected critical locations (Fig. 8) having relatively closer distance from valley slope surface. Considering this, 11 different locations are selected and cross-sections are drawn along the section lines as indicated in Figs. 8 and 9. The geometrical parameters required for the confinement criteria are measured from the cross-sections after the topographic correction is applied. In addition, Eqs. 7 and 8 are used in the area with multiple valley slopes. All necessary geometrical parameters needed for the analysis are listed in Table 7.

In Table 7, the factors of safeties calculated at different locations between T3 and T4 of the NEW HRT alignment are more than 3.5, which is well above the required factor of safety needed for the successful operation of the unlined/shotcrete lined pressure tunnel. One should note the fact that the confinement criteria consider only two parameters, i.e., the unit weight of the rock mass and geometry of the topography. Therefore, it is important that the other rock engineering issues, such as assessment on the in situ rock stress state, hydrogeological, and rock mass quality conditions, play crucial roles for the successful implementation of unlined/shotcrete lined pressure tunnels.

Rock engineering assessment

According to Nilsen and Palmstrom (2000), rock engineering assessment includes both rock mechanical behavior and engineering geological investigations. Regarding rock mechanical behavior, the strength and deformability of the rocks are important parameters to be estimated in order to use the rock mass as a natural concrete in unlined/shotcrete lined tunnels (Panthi 2014). The rock mass should be strong enough so that the water pressure does not break the rocks in the tunnel periphery. In reality, mineral content and its orientation in the rock mass determine the rock mass strength. In many rock formations of the Himalaya, schistosity is developed in the rock mass due to a medium to high degree of metamorphism. The schistosity creates

Table 6 Comparison of OLD HRT of UTHP with Norwegian projects (information on Norwegian cases based on Basnet and Panthi 2018a)

Category	Byrte	Askara	Fossmark	Nye Tyin	OLD HRT @ UTHP
Topography	Steep valley slope ($\beta = 41^\circ$), unlined shaft located close to valley slope	Two steep slopes in two different directions, unlined tunnel is about 150 m above valley bottom	Relatively steep slope, deep fjord valley, tunnel is about 350 m above fjord bottom	Gentle slope topography, tunnel is located far away and well below valley bottom	Multiple steep valley slopes, tunnel is located at about 300 m above deepest valley bottom
Rock mass and Jointing	Precambrian Granitic gneiss rock, two main joint sets with random joints, joints are filled with silt and clay	Devonian sand stone, two distinct joint sets, i.e., foliation and steeply dipping cross joints filled with silt and clay	Precambrian granitic gneiss, two distinct joint sets, steeply dipping toward and away from valley slope, joints are open to be filled with silt and clay	Precambrian dark gneiss in the high pressure part of the tunnel, joints are tight due to high confinement	Precambrian schistose gneiss, three joint sets and random joints, joints are open to be filled with silt and clay
Faults and weakness zones	Two weakness zones and one big fault called 'Byrte fault'	A crushed zone separates fractured rock mass with massive one	A distinct weakness zone across the reservoir lake strike parallel to the fjord valley	No nearby fault and weakness zones	Major weakness zones along Tamakoshi and Gongar valleys, shear zones crossing the tunnel alignment
In situ stress state	More than two thirds of the upper section of the shaft is located in the de-stressed area, S_3 is not always more than water pressure	Stress attenuated toward both steep slopes, de-stressing in the fractured sandstone above crushed zone, S_3 is less than water pressure at outer reach of the tunnel	Stress attenuation due to deep fjord valley, destressing due to the weakness zone, S_3 is less than water pressure in most locations of unlined shaft and tunnel	High confinement below the valley bottom due to high horizontal stress, S_3 is always greater than water pressure	Stress attenuation toward the valley slopes, de-stressing due to major weakness zones and shear zone, S_3 is less than water pressure in outer reach of the tunnel
Hydrogeology	Potential GWT is well below HWL in most parts of the unlined shaft	Potential GWT is well below HWL in outer reach of unlined tunnel	Potential GWT is always below the HWL	Potential GWT is fairly close to HWL	Potential GWT is well below the HWL, especially during dry period of the year

anisotropy in the rock strength and the rock strength is lower in another direction than that perpendicular to the

schistosity plane. Similarly, the geological features, such as major weakness and shear zones, jointing and

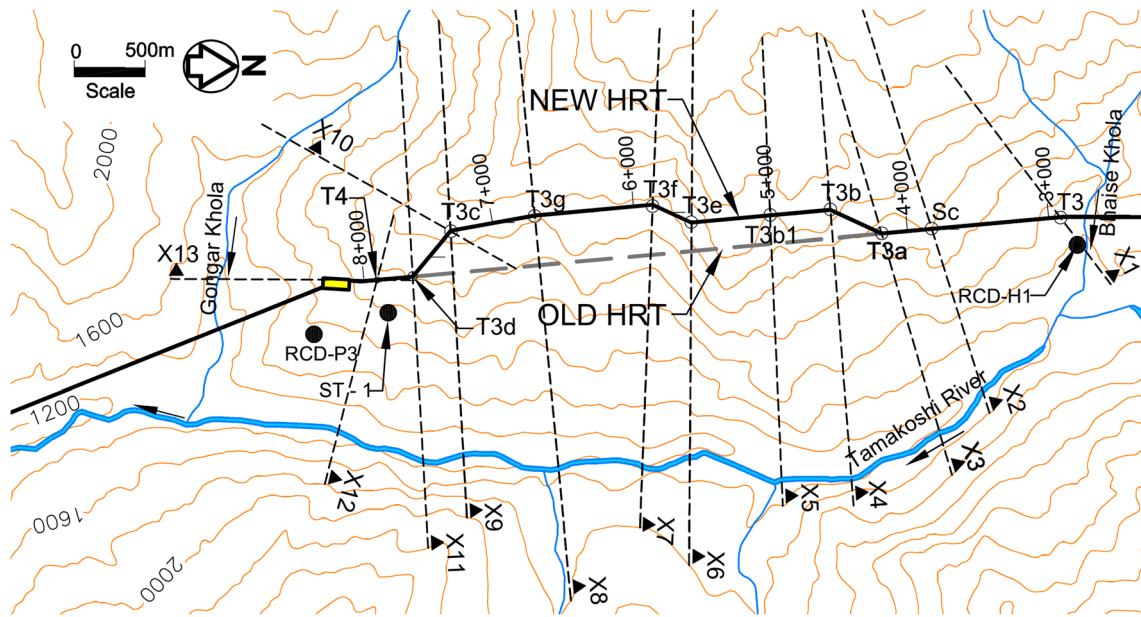


Fig. 8 Typical section lines at the selected critical locations along the NEW HRT of the UTHP

weathering conditions in the rock mass, ground water condition and in situ stress state, have to be assessed carefully. In order to assess the rock engineering aspect of the UTHP, surface, subsurface, and laboratory investigations were carried out. In addition, the exact information along the excavated tunnel gives a real database for such assessment. The identification of potential weakness zones and water

bearing joints at the surface and at the excavated tunnel are important parts of the assessment.

Surface investigation

The overall view of the topography and geological features, such as jointing, weakness zones, and shear zones, at the

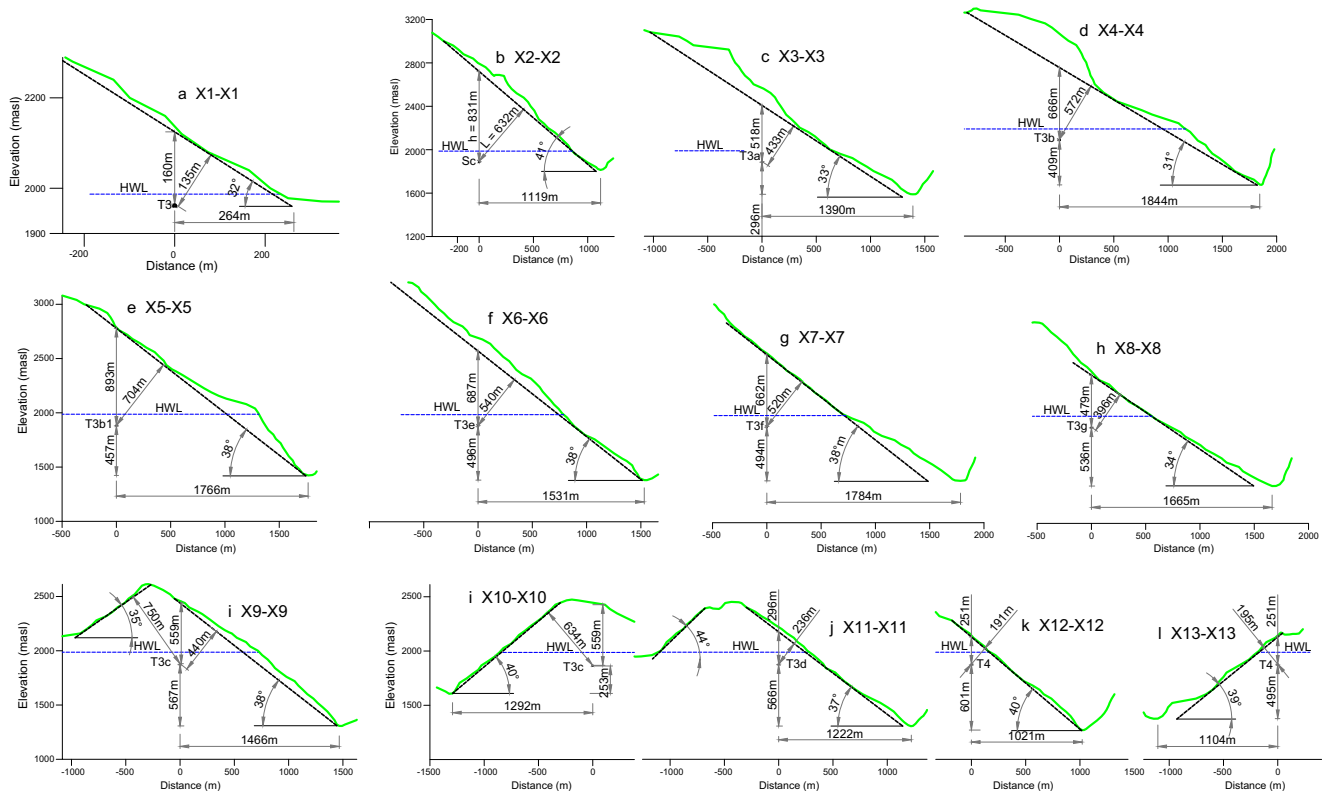


Fig. 9 Cross-sections across the tunnel alignment at different selected locations

Table 7 Analysis of the NEW HRT of the UTHP using confinement criteria

Location	H m	P_w MPa	γ_r MN/ m ³	h m	α Deg.	β Deg.	L m	$L\cos\beta$ m	FoS ₁	FoS ₂
T3	28	0.27	0.027	160	0	32	135	114.5	15.73	11.25
Sc	103.4	1.01	0.027	831	0	41	632	477.0	22.12	12.70
T3a	104.7	1.03	0.027	518	0	33	433	363.1	13.62	9.55
T3b	105.8	1.04	0.027	666	0	31	572	490.3	17.33	12.76
T3b1	107	1.05	0.027	893	0	38	704	554.8	22.98	14.27
T3e	108.7	1.07	0.027	687	0	38	540	425.5	17.39	10.77
T3f	109.6	1.08	0.027	662	0	38	520	409.8	16.62	10.29
T3 g	112.2	1.10	0.027	479	0	34	396	328.3	11.75	8.06
T3c	114	1.12	0.027	559	0	38	440	346.7	13.49	8.37
T3d	115.3	1.13	0.027	296	0	37	236	188.5	7.07	4.50
T4	115.4	1.13	0.027	251	0	40	191	146.3	5.99	3.50

Tamkoshi project area were observed from the left bank of the Tamakoshi valley and the right bank of the Gongar valley (Fig. 10). In addition, the detailed geological features were

identified and mapped along the road cuts and natural rock exposures at the surface. During mapping, emphasis was given to assess the features that cross cut the NEW HRT alignment

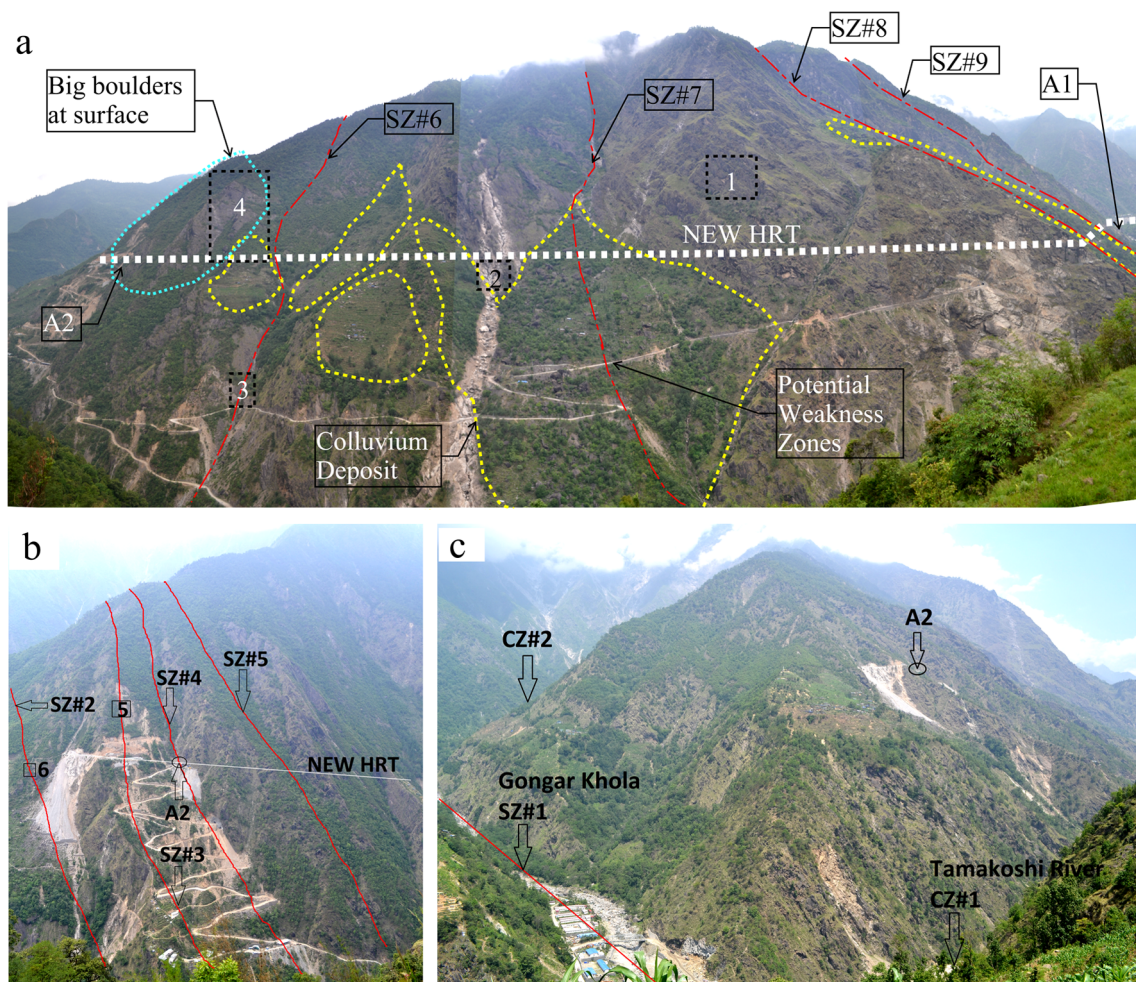


Fig. 10 a Overlaying of different information in the photo; b Potential shear zones at the outer reach of HRT overlaid in the photo, c Major river valleys representing the weakness zones and 3D topography at the outer reach of HRT (Note: all three photos were taken from left bank of the Tamakoshi River)

(Fig. 10a). The potential weakness zones were identified and their orientations were mapped. The weakness zones that are close to parallel to the foliation are identified as shear zones as defined by Panthi (2006) and Basnet and Panthi (2018b). In addition to the weakness zones, the jointing at road cuts and natural rock exposures were mapped in great detail. Potential ground water flow locations (local springs) were traced and identified. It is emphasized that in the areas where thick colluvium deposit and vegetation are present the ground water will percolate and expose at surface far below the potential leakage locations. Hence, a careful observation was necessary to identify the potential leakage locations at the surface.

As seen in the photos shown in Fig. 10b and c, the rock mass at the outer reach of headrace tunnel (downstream stretch) is schistose and fractured near surface and occurrence of weakness/shear zones are frequent. In addition, there exists complex topography with multiple slope directions due to river confluence and high relief toward both valleys (Tamakoshi valley on the right and Gongar valley on the left sides in Fig. 10c). The overall surface investigation showed that the outer reach of the headrace tunnel is more risk prone regarding the possibility of hydraulic jacking and consequent leakage compared to the upstream reach of the headrace tunnel where rock mass is relatively massive and less jointed. In this regard, a thorough rock engineering investigation is carried out along the NEW HRT alignment between the points T3 and T4 where static water head will be between 30 m and 115 m.

Mineralogy, strength, and deformability properties

The texture of the rock, which is exposed at the surface, can be seen in the photos in Fig. 11a and b. Figure 11a shows that the

rock mass is foliated, and Fig. 11b on the other hand shows relatively intact rock mass. The rock mechanical test was carried out at different stages of the project (Basnet and Panthi 2018b). The authors tested the rock samples collected during field mapping carried out in 2014 and 2016. The rock samples tested by the authors were extracted from the bore hole 'ST-1', but from different depths to represent overall rock mass (Fig. 11c). The rock cores have a diameter of about 50 mm, which is the same as that recommended by ISRM standard for different tests (ISRM 1978a, b; Bieniawski and Bernede 1979). The length and other dimensions of the samples were prepared according to the ISRM standards.

The tests were carried out in the rock mechanical laboratory at NTNU, Norway. The uniaxial compressive strength (UCS) and elastic modulus of nine rock cores were tested. Seven discs were prepared and tested to find tensile strength using the Brazilian test. In addition, other rock mechanical properties, such as unit weight and sound velocity, were also determined. Table 8 lists the statistical distribution of the tested parameters consisting of UCS (σ_{ci}), modulus of elasticity (E_{ci}), Poisson's ratio (ν), unit weight (γ_r), sound velocity (V_s), and tensile strength (σ_t). In the table, ' Δ ' is an angle between the schistosity plane and the loading direction. During the UCS test, failure occurred along the schistosity plane in most of the tested cores.

Panthi (2006) illustrated that the uniaxial compressive strength of intact rock specimen is smallest when the schistosity plane is inclined at around 30 degrees from the loading direction. In the tested samples of intact rock of the UTHP, the average angle is about 31 degrees, which means that the UCS values obtained from the laboratory test should be very close to the minimum possible strength. Table 8 shows that both compressive and tensile strengths of the tested intact

Fig. 11 a, b Typical rock exposures at surface locations c Rock samples collected from UTHP site, d typical rock core prepared for UCS test, e fractured core after UCS test, f typical cylindrical disc prepared for Brazilian tensile strength test, g fractured disc after Brazilian test

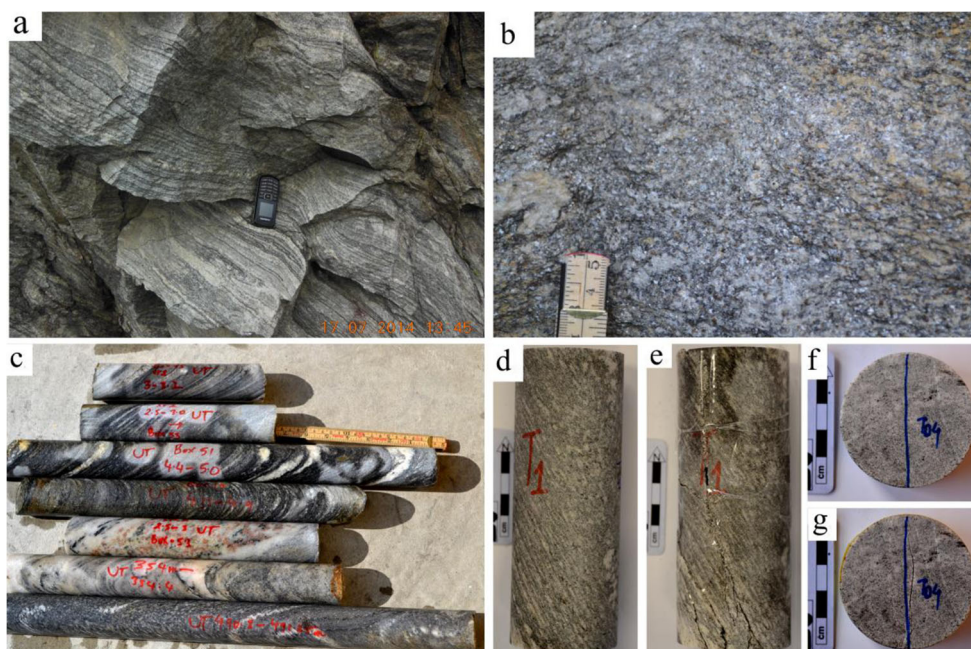


Table 8 Rock mechanical parameters of selected rock samples obtained from laboratory test

Statistical value	σ_{ci} MPa	E_{ci} GPa	ν	Δ deg	γ_r KN/m ³	V_s m/Sec	σ_t Mpa
Min.	61.5	33.5	0.1	22	26.4	4295	9.0
Mean	110.1	47.2	0.2	31	26.8	4736	10.0
Max.	182.6	60.4	0.3	35	27.8	5242	12.3
Sd.	39.9	8.1	0.06	4	0.40	321	1.2

rock of the UTHP are high enough compared to the water pressure at the tunnel. This indicates that the intact rock itself is not vulnerable to the hydraulic fracturing. However, the schistosity developed owing to weak minerals could make it vulnerable to hydraulic jacking.

The strength anisotropy of the rocks is mainly dependent on the mineralogical composition of the tested rock samples. Hence, altogether 11 rock samples were used for mineralogical analysis. The statistical distributions of the percentage of different minerals are listed in Table 9. The percentage of quartz exceeds 60% in most of the tested samples and the remaining minerals are represented by mica, biotite/muscovite, chlorite, graphite, and talc.

Rock mass quality along the NEW HRT

The rock mass quality along the headrace tunnel was mapped during tunnel excavation and rock mass quality registration was mainly carried out using the Q-system as defined by Barton et al. (1974). The six parameters of Q-value are listed in Table 10 with their statistical range for each of the particular rock mass quality classes registered along the headrace tunnel. As one can see in Table 10, the rock mass quality along the tunnel varies from good (Q-value exceeding 4.0) to very poor (Q-value less than 0.1) rock mass class. In the hard rock, the Q-values in the fractured or jointed rock mass fall between the ranges of 0.1 to 4.0. On the other hand, the Q-values of the crushed, weathered, and clay mixed rock mass of the weakness zones fall below 0.1, representing the extremely poor to exceptionally poor rock mass category.

Figure 12 shows rock mass quality mapped along the new alignment (NEW HRT) of the headrace tunnel between chainage 2 + 914 m (T3) to chainage 7 + 860 m (T4). As one

can see, almost four-fifth of the length of the headrace tunnel has good quality rock mass. However, about 700 m of the mapped headrace tunnel has fractured rock mass and approximately 200 m of the tunnel stretch meets the rock mass of the weakness zones. It is especially noted that the rock mass at the downstream end of the headrace tunnel (Downstream from chainage 7 + 300 m) where the static water pressure will reach its maximum of 1.15 MPa is mainly dominated either by fractured rock mass or by the rock mass of the weakness zones.

The three different groups of rock mass indicated in Fig. 12 behave differently when exposed to high water pressure. The good quality rock mass are relatively resistive toward the hydraulic fracturing/jacking if the minimum principal stress is higher than the static water pressure. However, the fractured rock mass are vulnerable to hydraulic jacking and leakage due to the presence of joints either open or filled with silty clay and sand. Similarly, the rock mass of the weakness zones are unfavorable for the unlined tunnels due to very low magnitude of minimum principal stress caused by local de-stressing.

Joints and their characteristics

The rock mass in the Tamakoshi area is foliated and schistose. The rock exposures seen at surface have at least three joint sets including foliation joints. The typical rock exposures at the cliff area and the road cut are shown in Fig. 13a and b. The orientations of the joint sets at the surface are presented by Panthi and Basnet (2017). During the surface mapping, the joints at the surface were found open or filled with silt and clay. Long persisting joints identified at the surface possibly communicate the joints mapped inside the tunnel. The typical joint sets along the tunnel wall and tunnel face are shown in Fig. 13c and d, respectively.

Table 9 Mineral composition of the rock samples

Statistical value	Mineral content in (%)											
	Quartz	Muscovite	Albite	Biotite and Mica	Microcline	Spessartine	Hornblende	Calcite	Meionite	Dolomite	Diopside	Siderite
Min.	62.82	0.95	1.80	0.36	2.57	0.33	1.29	0.74	–	–	–	–
Mean	72.12	5.79	10.35	1.82	9.60	4.25	1.98	0.78	11.21	0.32	0.80	1.02
Max.	88.95	13.44	14.44	2.52	15.01	6.87	2.66	0.82	–	–	–	–
Sd.	7.97	4.31	4.11	0.63	4.70	2.83	0.69	0.04	–	–	–	–

Table 10 Rock mass quality along the HRT based on *Q-value

Rock mass quality	Statistical value	Rock mass parameters						
		RQD	J _n	J _r	J _a	J _w	SRF	Q-value
Good quality rock ($Q \geq 4.0$)	Min.	35	3	1.0	0.8	0.3	1.0	4.03
	Mean	72	6	1.8	2.2	1.0	1.1	10.51
	Max.	98	12	3.0	6.0	1.0	2.5	65.33
	Sd.	17	2	0.7	0.8	0.1	0.4	7.41
Fractured rock ($0.1 < Q < 4.0$)	Min.	15	3	0.5	1	0.33	1	0.10
	Mean	53	9	1.6	3.3	0.9	1.9	1.92
	Max.	90	18	3.0	8.0	1.0	5.0	3.89
	Sd.	17	3	0.6	1.6	0.2	1.1	1.03
Weakness Zone ($Q \leq 0.1$)	Min.	10	9	0.5	5.0	0.7	2.5	0.01
	Mean	26	18	1.0	8.4	0.9	8.6	0.02
	Max.	65	20	1.0	10.0	1.0	10.0	0.06
	Sd.	13	5	0.1	1.0	0.1	2.1	0.02

* $Q = RQD/J_n \cdot J_r/J_a \cdot J_w/SRF$

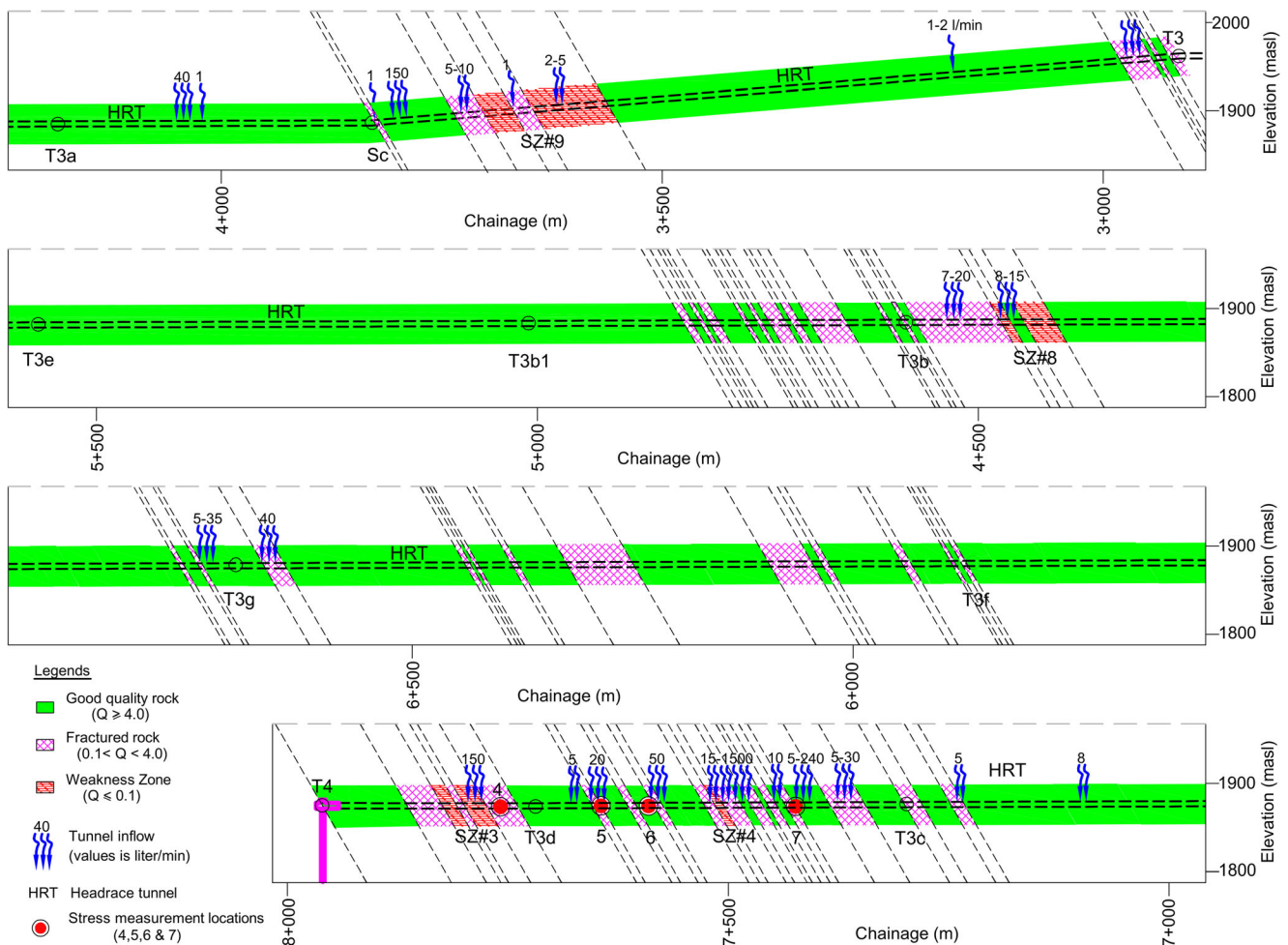


Fig. 12 Rock mass quality and inflow along the headrace tunnel (NEW HRT) registered during excavation

Fig. 13 Jointing at different locations: **a** Jointing seen on the cliff (photo 1 in Fig. 10a), **b** Jointing at road cut hill side (photo 3 in Fig. 10a), **c** Open joint at tunnel wall; **d** Jointing at tunnel face at the area of relatively good quality rock mass

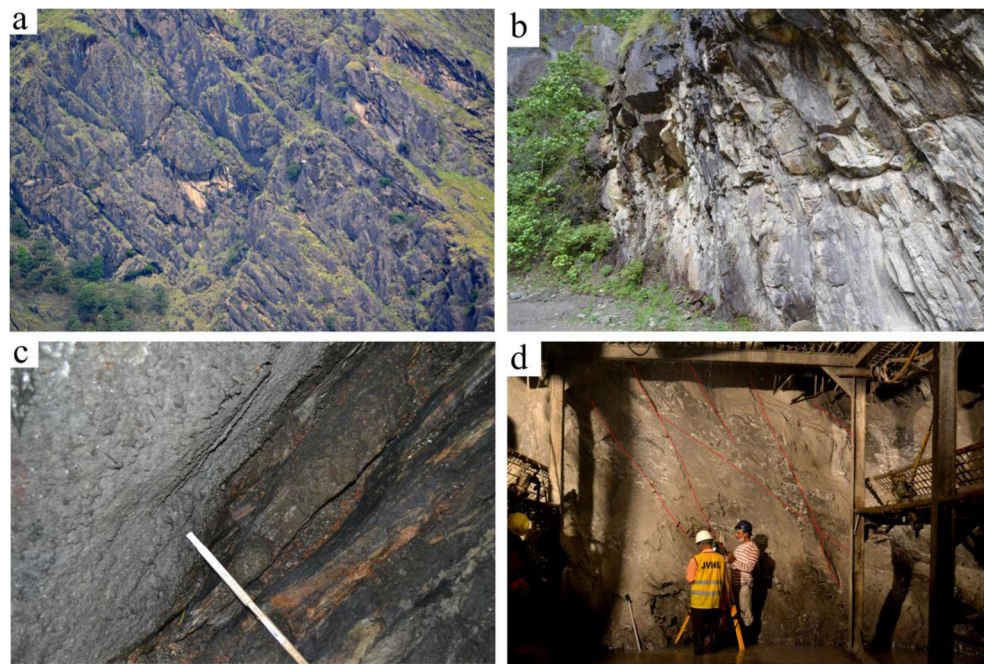


Figure 14 presents the orientation of joints in stereographic projection (Fig. 14a) and joint rosettes (Fig. 14b, c and d). The overall jointing pattern along the mapped tunnel stretch between T3 and T4 is represented by three distinct joint sets and some random joints (Fig. 14a). The jointing patterns for three different categories of rock mass discussed above are presented separately in Fig. 14b, c, and d. As one can see in the figures, the good quality rock masses have mainly two prominent joint sets. The mapped joints found along the tunnel are mostly tightly healed and intact, excluding some crossed joints that are filled with silty clay with a thickness 1 to 2 mm. In addition, quartz and feldspar veins of up to 20 cm thick are also occasionally glued within the foliation joints. The fractured rock mass on the other hand has three to four distinct joint sets plus random joints (Fig. 14c). The rock mass in this category consists of mainly the joints filled with permeable silty clay of thickness exceeding 10 mm. This thickness reaches 100 mm in those areas of the rock mass where local shear bands are developed along the foliation plane. In the cases of the weakness zones, it was difficult to map distinct joint sets due to the fact that the rock masses here are completely crushed. Despite this, some distinct joint sets were mapped and their main orientations are presented in Fig. 14d.

Near surface de-stressed areas

The colluvium deposits shown in Fig. 10 are almost de-stressed and weathered material. The large cracks and big boulders observed at the surface as shown in Figs. 10 and 15a and b are mainly due to de-stressing caused by stress anisotropy. It is emphasized here that these de-stressed areas are mostly located at the

outer reach of the headrace tunnel alignment. It is logical to infer that both colluvium deposits and de-stressed boulder blocks have very small contributions in the in situ stress state at the tunnel location. The de-stressing effect due to such deposits depends upon the depth of the deposits from the surface. It is very difficult to estimate the depth of many of these areas due to limited accessibility at the surface caused by steep topography. Nevertheless, the logged information from boreholes ‘ST-1’ and ‘RCD-P3’ indicated that the weathering depth continued maximum up to 25 m from the surface. The mapped material at borehole ‘RCD-H1’ located at the right bank of Bhaise Khola indicated that the completely weathered rock material continued all the way up to a 48 m depth from the surface (Panthi and Basnet 2017). On the basis of the bed rock exposures at the surface and information from the borehole, it is concluded that the weathering depth along the headrace tunnel varies between 10 m to 50 m in depth.

Weakness zones

Potential weakness zones were marked at the surface as shown in Fig. 10. The major weakness zones along the Tamakoshi valley and upper part of the Gongar valley are represented by the crushed zones (Basnet and Panthi 2018b). In addition, one of the major weakness zones along the Gongar valley near the Tamakoshi valley is a shear zone. Some weakness zones were also marked at the surface along the headrace tunnel alignment as shear zones. A distinct shear zone that is exposed at the surface near the shaft area is shown in Fig. 15c. This zone demarcates two different rock qualities. On the left side of the demarcation line (red color) in Fig. 15c, the rock mass is jointed but relatively stronger than the rock mass on the right

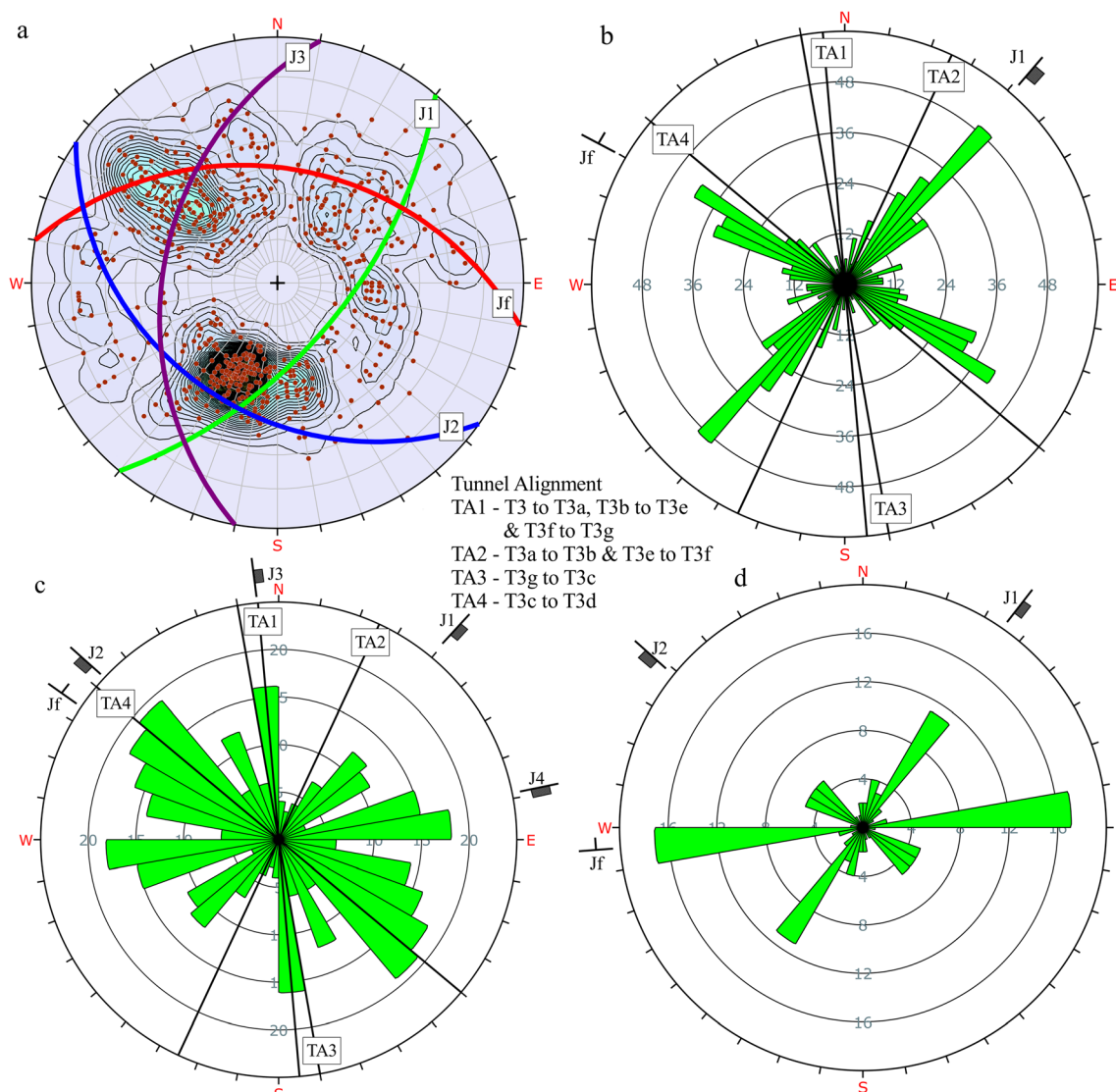


Fig. 14 Orientation of joints and tunnel alignment; **a** Overall jointing pattern along HRT from T3 to T4 (stereographic equal angle projection, lower hemisphere), **b** Joint rosette in good quality rock mass, **c** Joint rosette in fractured rock mass and **d** Joint rosette in weakness zones

side of the line, which is crushed and disintegrated. Altogether, eight distinct shear zones were identified at the surface in the area between Bhaise Khola and Gongar Khola.

Some distinct weakness zones were also mapped along the tunnel during excavation (Fig. 12). One such zone encountered while tunneling is shown in Fig. 15d. The shear zones identified in the surface topography, such as SZ#3, SZ#4, SZ#8, and SZ#9, can be easily extrapolated to match the respective shear zones mapped along the NEW HRT alignment. Similarly, the possible location of SZ#2 was mapped at the upper penstock shaft and the OLD HRT. The shear zones are oriented more or less parallel to the foliation joints, while the crushed zones are striking parallel to the river valleys and steeply dipping (Basnet and Panthi 2018b). The orientation of all crushed and shear zones are presented in a stereographic projection as shown in Fig. 16.

Weathering conditions

According to Panthi (2006), rock weathering has great influence on the strength and deformability properties of the rock mass. The extent of influence depends on the degree of weathering. The degree of weathering observed along the headrace tunnel alignment is categorized into five different weathering classes according to ISRM (1978c), and their frequency distribution is presented in Fig. 17.

In the figure, 'N' is total number of mapped tunnel segments. As one can see in the figure, the rock mass along the tunnel alignment falls within the slightly weathered class (II) category representing good to very good rock mass quality. The fractured rock mass mainly falls within the moderately weathered class (III) category and the rock mass in the weakness zone falls in the highly weathered to extremely weathered class (IV) category.

Fig. 15 **a** Big boulders and open cracks seen on the surface (photo 4 in Fig. 10a); **b** Approx. 1 m wide crack seen on the surface (photo 6 in Fig. 10b); **c** Typical weakness zone at surface (photo 5 in Fig. 10b); **d** Weakness zone at the HRT (photo credit: UTHP); **e** Typical weathering condition of rock mass at surface; **f** Typical weathering condition inside tunnel; **g** Typical rivulet at surface topography at about tunnel level (photo 2 in Fig. 10a); **h** concentrated tunnel inflow of about 1500 l/min at 7 + 487 m chainage inside the HRT (Photo credit: UTHP)



According to Panthi (2006), the degree of weathering greatly influences the strength and modulus of elasticity of the intact rock. Figure 17 shows the respective reduction percentage for each weathering grade based on Panthi (2006).

Inflow registration during excavation

The water bearing areas at the project area are mostly localized along the rivulets and rivers. A typical rivulet crossing the

headrace tunnel alignment has distinct joint sets, as can be seen in Fig. 15g. The headrace tunnel crosses over eight such rivulets (Fig. 10). These rivulets are the main source of ground water that seeps into the tunnel through permeable joints. A typical water inflow into the headrace tunnel is shown in Fig. 15h. Through these inflow paths, water may also leak during plant operation if the ground water pressure is below that of the hydro static water head. Hence, tunnel inflow registration gives crucial information regarding potential water leakage out of the tunnel during the

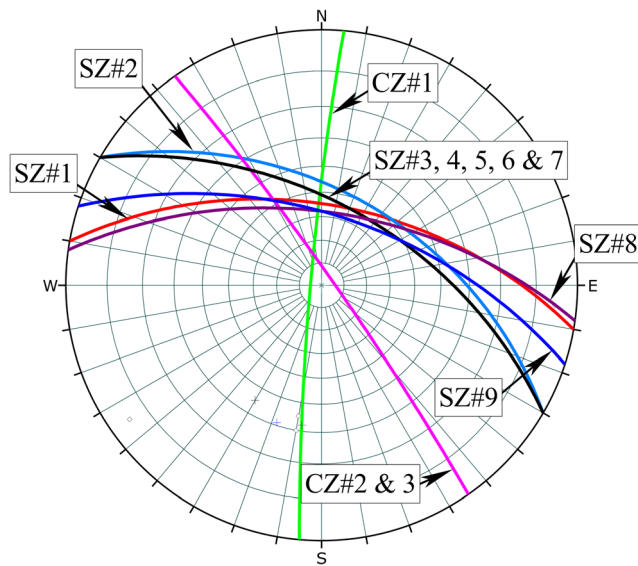


Fig. 16 Orientation of potential weakness zones (equal angle, lower hemisphere)

operation phase. In Fig. 12, some typical inflow locations are indicated along the tunnel with the approximate amount of tunnel inflow registered during tunnel mapping. Most of the inflow was registered at the area of fractured rock mass with the highest inflow of about 25 l/s (Fig. 15h).

Stress state assessment

The rock engineering data and stress measurement data of the UTHP area are essentially valuable information while evaluating the in situ stress state. However, these data represent specific locations and may mislead the result if directly used for the interpretation of larger rock volume (larger topographic coverage). In order to integrate these data for the analysis of stress state of quite a large rock volume of the UTHP area, a final rock stress model (FRSM) concept as recommended by Stephansson and Zang (2012) is extensively utilized (Table 11).

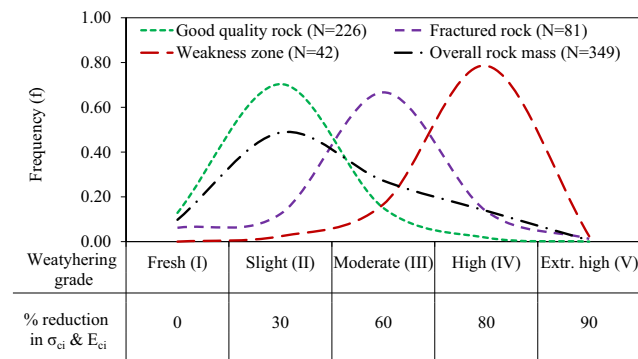


Fig. 17 Weathering grade of rock mass with different qualities and percentage reduction in intact rock strength and modulus of elasticity (modified from Panthi 2006)

Table 11 Formulation of final rock stress model applicable to the UTHP based on Stephansson and Zang (2012)

Best Estimate Stress Model BESM	Stress Measurement Methods SMM	Integrated Stress Determination ISD	Final Rock Stress Model FRSM
<ul style="list-style-type: none"> Information on topography, tectonics, geology, lithology, etc. 	<ul style="list-style-type: none"> Hydraulic fracturing (HF) 3D overcoring (OC) 	<ul style="list-style-type: none"> ISD model Hydraulic fracturing (HF) 3D overcoring (OC) Numerical modeling Numerical model (FLAC^{3D}) 	<ul style="list-style-type: none"> Best-fit model Final result: magnitude of minimum principal stress

By virtue of its complexity in topography and geo-tectonics, the UTHP area is analyzed by generating a FRSM for a reliable stress state estimation. The FRSM concept considers stepwise evaluation of the in situ stress state integrating best estimate stress model (BESM), stress measurement methods (SMM), and integrated stress determination methods (ISD). Stephansson and Zang (2012) concluded that the resulting stress data are more relevant for larger rock volume after the ISD model and stress modeling are performed. Hence, both the ISD model and numerical analysis (FLAC^{3D} model) are used to develop the final rock stress model for the UTHP case. Four basic steps are followed to develop the FRSM. First, three dimensional geometry inside the model extent is generated in FLAC^{3D}, where the model extent is chosen in such a way that it covers the stretch of pressure tunnel from T3 to T4 as well as the stress measurement locations. Second, input parameters to the model are defined and uncertainties of different parameters are evaluated with the help of information gathered from the Tamakoshi area; the BESM established by Basnet and Panthi (2018b) for the Tamakoshi area is extensively used. Third, the global misfit function is defined to express the discrepancy between the measured and the predicted stresses by integrating the result from both 3D overcoring and hydraulic fracturing techniques. Fourth, the global misfit is minimized to generate the best-fit model. The output from the best-fit model is considered to be a best possible result for the NEW HRT alignment of the project.

FLAC^{3D} model

In FLAC^{3D} software, the differential equations that describe the mechanical behavior of the rock mass are solved with the explicit finite difference method (ITASCA 2017). The major calculation steps in FLAC^{3D} involve: (a) nodal forces are calculated from the loading, such as stresses, body forces, etc., (b) the equations of motion are used to derive new nodal

velocities and displacements, (c) new strain rates are derived from nodal velocities, (d) constitutive equations are used to calculate new stresses from the strain rates and stresses at the previous time, and (e) the equations of motion are again used to derive new nodal velocities and displacements from stresses and forces. These calculation steps are repeated at each cycle until the maximum out-of-balance force approach to zero indicating that the system is reaching an equilibrium state. Nevertheless, the geometry, material properties, boundary, and initial conditions should be well defined before the execution of these calculation steps. The Tamakoshi project area consists of a single rock type, i.e., schistose gneiss. For simplicity, the rock mass is considered as a homogeneous and isotropic material even though the rock mass possess some degree of anisotropic behavior because of the schistosity. The constitutive equations derived for a linearly elastic model is used where the material is expected to exhibit linear stress-strain behavior. The authors strongly believe that these assumptions are representative enough in this study since the objective is to find the in situ stress state for a large area.

Geometry

The area of interest for the NEW HRT alignment of UTHP is toward the north from Gongar Khola and toward the west from the Tamakoshi River (Fig. 18a). The north-south extent of the area of interest is the NEW HRT between T3 and T4 and the locations of stress measurement. Similarly, the westward extent of the area of interest is up to the stress measurement locations by hydraulic fracturing. Keeping this in mind, a model extent is defined with an aerial size of 5500 m X 7500 m (Fig. 18a). While defining the model extent, the model boundary is located

in such a way that the influential stretches of both Tamakoshi and Gongar valleys to the area of interest lie well inside the model extent. Within the model extent shown in Fig. 18a, a 3D geometry is generated with the help of the building blocks option in FLAC^{3D}. The generated 3D geometry is shown in Fig. 18b, which incorporates the topography shown in Fig. 18a. Positive Y-axis of the geometry as shown in Fig. 18b is aligned toward the north. The bottom of the model is fixed at -1000 masl. The depth of the model varies according to the topography inside the model extent. The major part of the geometry is meshed with finer brick shaped elements in the area of interest and the size of the elements is coarser toward the boundaries away from the area of interest. In addition, both wedge and tetrahedral shaped elements are used to fill the geometry in the rest of the irregular places. The meshes in the geometry are shown in Fig. 18b. In the model, 1,177,631 three dimensional elements are generated in total. In addition, all potential weakness zones are created as interfaces in 3D geometry as shown in Fig. 18b. The figure shows that there are altogether 12 weakness zones (both crushed and shear zones) within the model extent. Furthermore, Fig. 19 shows how the grids and interfaces are generated inside the model extent. One can clearly see in the figure that the 3D elements are finer at the area where the headrace tunnel is located.

Input parameters

Rock mass parameters are required as input to define the rock mass behavior, while the interface parameters are used to define the behavior of weakness zones. The input parameters required for the model are quantified on the basis of the detail mapping, information received from Tamakoshi project, and laboratory testing. Table 12 shows the mean values (with

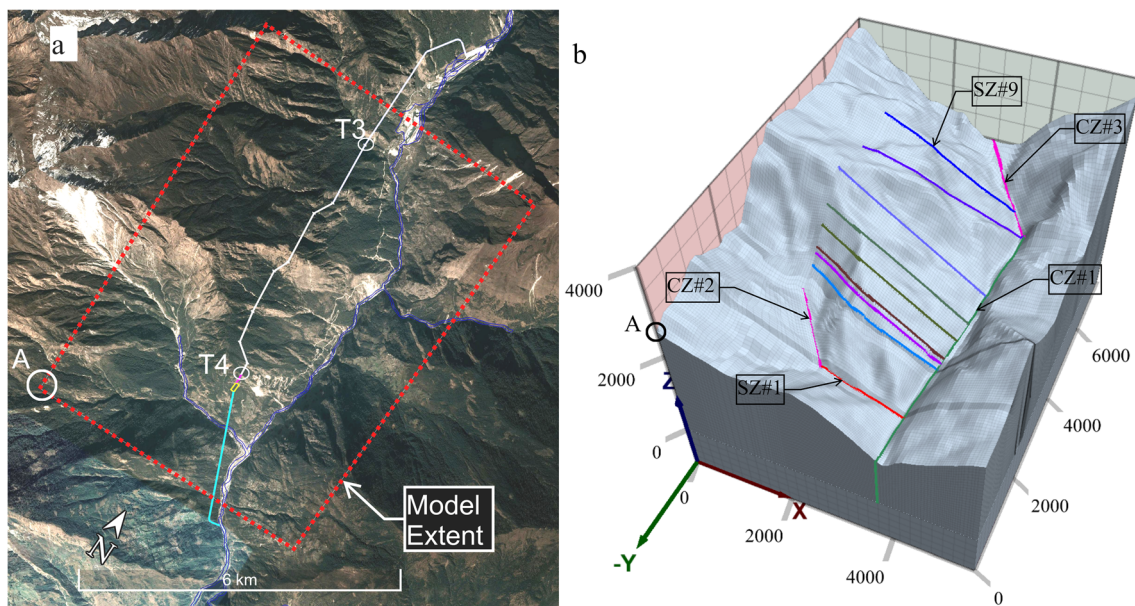


Fig. 18 a Model extent overlaid in the map of the UTHP area (source: www.earth.google.com); b 3D geometry built in FLAC^{3D} with grids and potential weakness zones (interfaces)

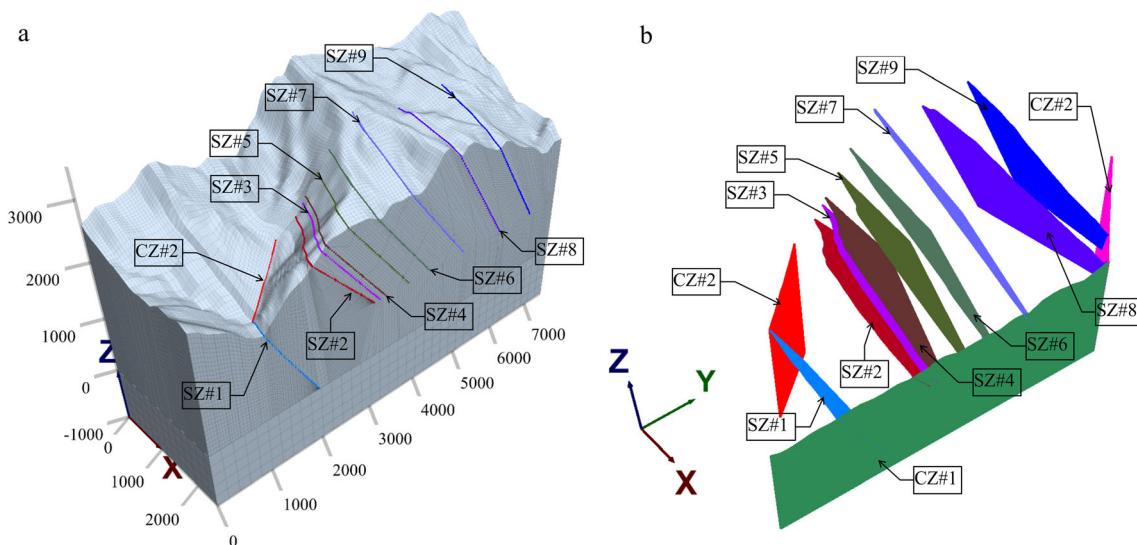


Fig. 19 a 3D geometry, grids, and interfaces along north-south section at X = 2500 m; b The interfaces in 3D

standard deviation) of uniaxial compressive strength of intact rock (σ_{ci}), modulus of elasticity of intact rock (E_{ci}), poisson's ratio (ν), and specific unit weight of the rock (γ_r) tested by the authors. The values are taken from Table 8. In addition, the table also shows the weathering grade and reduction percentage as defined in Fig. 17 for overall rock mass along the headrace tunnel. The reduced values of σ_{ci} and E_{ci} are used to calculate the bulk modulus (K) and shear modulus (G) using the relationship given by Goodman (1989) for isotropic rock material. The bulk modulus (K), shear modulus (G), and specific unit weight (density) of the rock are input to FLAC^{3D} for the linearly elastic constitutive model.

Furthermore, all 12 weakness zones are modeled as interfaces. The interface parameters, such as stiffness and friction angle, are important parameters to FLAC^{3D}. Stiffness of the weakness zone depends on the elasticity properties and thickness of the zone

material. Usually, both normal and shear stresses are acting on the weakness zone as shown in Fig. 20. In the figure, S_n is normal stress and S_s is shear stress and E_0 and G_0 are Young's modulus and shear modulus of weakness zone material, respectively. The normal (k_n) and shear (k_s) stiffness of the weakness zones can be estimated if the values of E_0 and G_0 are known in addition to the thickness of the zone (t). The relationships are shown in Fig. 20, which were also used by Li et al. (2009) in their analysis.

The Young's modulus of the material at the weakness zones is considered equal to the deformation modulus of the rock mass of that zone. Three different approaches are used to calculate the deformation modulus of the weakness zone material (Barton 2002; Hoek and Diederichs 2006 and Panthi 2006). Different parameters and relationships used in the calculation are given in Table 12. Barton (2002) used the mapped Q-value and the UCS value in his relationship. On

Table 12 Properties of gneiss/schist of the UTHP

Rock condition	Parameters	Unit	Statistical values	
			Mean	Sd
Intact rock	Unit weight ^a , γ_r	KN/m ³	26.8	0.40
	Poisson's ratio ^a , ν		0.20	0.06
	Elasticity modulus ^a , E_{ci}	GPa	47	8
	Intact rock strength ^a (UCS), σ_{ci}	MPa	110	40
Weathered rock	Weathering grade		II	–
	Reduction in UCS and E_{ci} , P_R	%	30	–
	UCS after correction, σ_{ci}'	MPa	77	28
	E_{ci} after correction, E_{ci}'	GPa	33	6
	Bulk Modulus ^b , K	GPa	18.4	3.2
	Shear Modulus ^c , G	GPa	13.8	2.4

^a laboratory test result

^b $K = E_{ci}' / (3(1 - \nu))$

^c $G = E_{ci}' / (2(1 + \nu))$

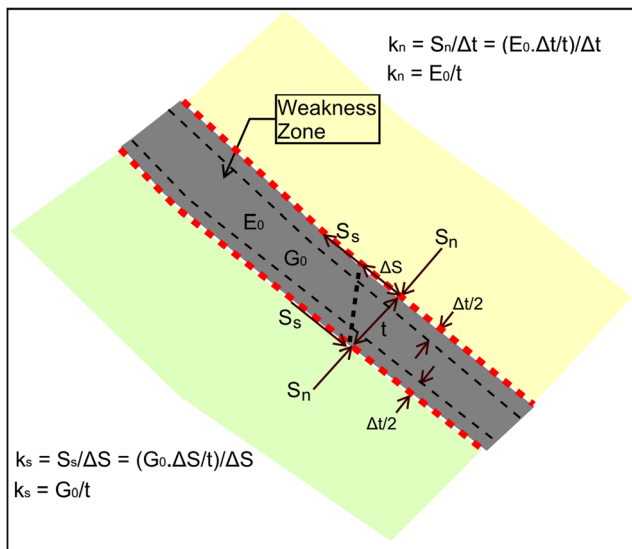


Fig. 20 Weakness zone in between the relatively stiff rock masses

the other hand, Hoek and Diederichs (2006) used GSI value, modulus of elasticity, and disturbance factor (D) in their relationship. To calculate the GSI value, the mapped Q-value is first transformed to RMR value by using the relationship suggested by Barton (1995) and then to GSI value by using the equation proposed by Hoek and Diederichs (2006). For the in situ condition, D is equal to zero. Furthermore, Panthi (2006) used both UCS and modulus of elasticity in his relationship. In all relationships, the reduced value of strength and modulus of elasticity after correction for weathering grades are used.

The tested UCS and young’s modulus of elasticity from Table 8, weathering grade of weakness zone, and mapped Q-values at weakness zones are used to calculate the modulus of elasticity of the rock mass at the weakness zones located along the NEW HRT alignment of the project. The statistical distribution of the modulus of elasticity of the weakness zone material in

Table 13 shows that Barton (2002) gives the upper limit of E_0 , whereas Hoek and Diederichs (2006) give the lower limit of E_0 . The mean value calculated from Panthi’s (2006) approach lies in between the mean values from the other two approaches. Since Panthi’s (2006) approach is relevant for the Himalayan region, it was decided to use this approach for the calculation of the mean value of E_0 for all eight shear zones located along the NEW HRT alignment. The properties of crushed zones ‘CZ#1’ and ‘CZ#2’ and shear zones ‘SZ#1’ and ‘SZ#2’ were already evaluated and optimized by Basnet and Panthi (2018b). The properties of crushed zone ‘CZ#3’ are assumed to be similar to that of the other two crushed zones. Friction angle of the interface is another important parameter to be estimated. Usually, it ranges from 15° to 30° in the case of fault/weakness zones (Barton 1973). Friction angle of 25° is estimated as the most likely value based on the observation and rock mass quality description of the shear zone met at the tailrace and headrace tunnels. All estimated interface parameters are given in Table 14.

Boundary and initial condition

Boundaries at east, west, north, and south faces are prevented for both normal and horizontal shear displacements to occur by fixing the corresponding velocities to zero values. The bottom face is prevented for normal displacement only. The assumption here is that the boundaries are located in such a way that the proximities of the boundaries do not influence the result at the area of interest. On the other hand, the surface topography is left free in order to generate the gravity loading to the area of interest. Since the boundaries are fixed, the stresses due to both gravity and tectonics are initialized in each element for whole geometry, which is one of the recommended solutions to evaluate the stress state in an undulating topography like the Tamakoshi area (ITASCA 2017). In the FLAC^{3D} model, both normal stresses and shear stresses are

Table 13 Modulus of elasticity of the material at weakness zone estimated by different approaches

Statistical values	σ_{ci} MPa	E_{ci} GPa	Weathering grade	P_R %	σ_{ci}' MPa	E_{ci}' GPa	Q	RMR ^a	GSI ^b	Q_c^*	Modulus of elasticity (E_0), GPa		
											^c Barton (2002)	^d Hoek and Diederichs (2006)	^e Panthi (2006)
Min.	61.5	33.5	–	90	6.2	3.3	0.007	17	12	0.001	1.0	0.2	0.2
Mean/most likely	110.1	47.2	IV	75	29.9	12.8	0.022	24	19	0.007	1.8	0.6	1.2
Max.	182.6	60.4	–	60	73.0	24.2	0.060	32	27	0.044	3.5	1.6	3.3
Sd.	39.9	8.1	–	–	13.1	3.7	0.014	3	3	0.008	0.5	0.3	0.6

* $Q_c = Q \times \sigma_{ci}' / 100$

^a $RMR = 15 \log Q + 50$

^b $GSI = RMR - 5$

^c $E_0 = 10 \times Q_c^{1/3}$

^d $E_0 = E_{ci}' \times (0.02 + (1-D)/2) / (1 + e^{((60 + 15D - GSI)/11)})$

^e $E_0 = 1/60 \times E_{ci}' \times \sigma_{ci}'^{(0.5)}$

Table 14 Weakness zone (interface) parameters

Interfaces	E_0	ν_0	G_0^a	t	k_n^b	k_s^c	Friction angle deg
	GPa		GPa	m	Pa/m	Pa/m	
CZ#1	1.6*	0.1	0.73	35	4.6E+07	2.1E+07	25
CZ#2	1.6*	0.1	0.73	25	6.4E+07	2.9E+07	25
CZ#3	1.6*	0.1	0.73	35	4.6E+07	2.1E+07	25
SZ#1	1.6*	0.1	0.73	25	6.4E+07	2.9E+07	25
SZ#2	1.6*	0.1	0.73	30	5.3E+07	2.4E+07	25
SZ#3	1.2	0.1	0.55	35	3.4E+07	1.6E+07	25
SZ#4	1.2	0.1	0.55	15	8.0E+07	3.6E+07	25
SZ#5	1.2	0.1	0.55	20	6.0E+07	2.7E+07	25
SZ#6	1.2	0.1	0.55	20	6.0E+07	2.7E+07	25
SZ#7	1.2	0.1	0.55	20	6.0E+07	2.7E+07	25
SZ#8	1.2	0.1	0.55	55	2.2E+07	9.9E+06	25
SZ#9	1.2	0.1	0.55	65	1.8E+07	8.4E+06	25

*Basnet and Panthi (2018b)

^a $G_0 = E_0 / (2(1 + \nu_0))$

^b $k_n = E_0 / t$

^c $k_s = G_0 / t$

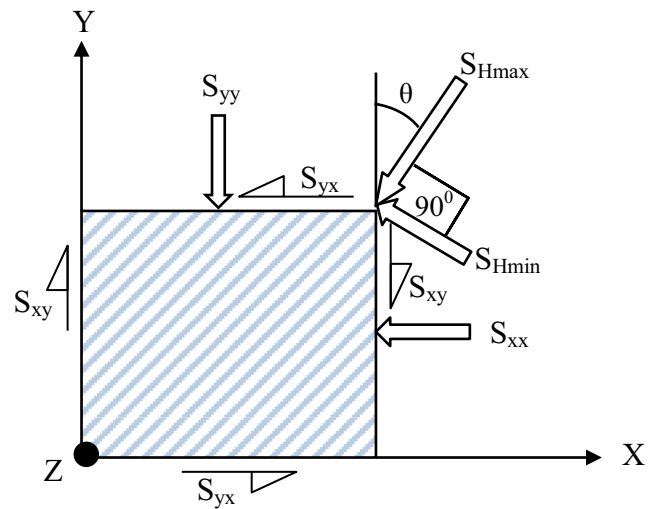
initialized in each zone. The normal stress along the Z-axis (S_{ZZ}) is mainly due to the vertical overburden (h) of the rock mass. A part of horizontal stress due to gravity acts hydrostatically because of the Poisson's effect of the rock mass. In addition, the total horizontal stresses are also contributed by tectonic stresses (Eqs. 10 and 11).

$$S_{Hmax} = S_{Tmax} + \frac{\nu}{1-\nu} S_{zz} \quad (10)$$

$$S_{Hmin} = S_{Tmin} + \frac{\nu}{1-\nu} S_{zz} \quad (11)$$

Where S_{Tmax} and S_{Tmin} are maximum and minimum tectonic stresses, respectively, and S_{Hmax} and S_{Hmin} represent respective maximum and minimum total horizontal stresses. Since the tectonic stresses are anisotropic, the corresponding total horizontal stresses are also anisotropic. Let us consider, S_{Hmax} makes an angle θ with Y-axis (north direction) as shown in Fig. 21 where the direction of S_{Hmin} is perpendicular to S_{Hmax} .

The normal stresses along Y- and X-axes are calculated by resolving S_{Hmax} and S_{Hmin} using Eqs. 12 and 13, respectively. Since the maximum horizontal stress makes an angle (θ) with Y-axis, there will be horizontal shear stresses in YZ and XZ

**Fig. 21** Resolving horizontal stresses in X and Y directions

faces as shown in Fig. 21 (the box shown in the figure has thickness along Z-axis). These shear stresses have the same magnitudes in both faces and are estimated by using Eq. 14.

$$S_{yy} = S_{Hmax} \cos^2 \theta + S_{Hmin} \sin^2 \theta \quad (12)$$

$$S_{xx} = S_{Hmax} \sin^2 \theta + S_{Hmin} \cos^2 \theta \quad (13)$$

$$S_{xy} = S_{yx} = \frac{S_{Hmax} - S_{Hmin}}{2} \sin 2\theta \quad (14)$$

The stresses, i.e., S_{xx} , S_{yy} , S_{zz} , and S_{xy} , are initialized in each zone of the 3D model. For simplicity, S_{zz} is assumed as one of the principal stresses, which means the shear stresses, S_{xz} (S_{zx}), and S_{yz} (S_{zy}), are essentially zero.

Definition and measurement of misfit

The misfit is a non-dimensional feature that signifies the differences between the observation and the calculated result (e.g., Parker and McNutt 1980; Revets 2009). The model is said to be optimized when the misfit becomes absolutely minimum. Different misfit functions such as l_1 -norm, l_2 -norm are used in practice. In the present analysis, the l_1 -norm is adopted for the measurement of misfit because of the simplicity in the calculation measure combined with its considerable robustness against outliers (Yin and Cornet 1994; Ask 2006 and Revets 2009). The misfit functions for both hydraulic fracturing and overcoring methods are first defined separately. For hydraulic fracturing data, the misfit is defined by Eq. 15.

$$\psi^{HF} = \sum_{m=1}^M \frac{|S_{mes1}^m - S_{cal1}^m|}{S_d^m} \quad (15)$$

Where S_{mes1} and S_{cal1} are the measured and calculated (simulated) principal stresses, respectively, S_d is the

uncertainty in principal stress measurements (standard deviation in the present case) and M is the total number of measured stress data by the hydraulic fracturing method. The principal stresses are used in Eq. 15 instead of the normal stress in the originally proposed equation by Ask (2006) and Figueiredo et al. (2014). The reason behind this is that the fracture delineation was not recorded in the tests conducted in the UTHP. Both minimum and maximum principal stresses are used to calculate the overall misfit (Eq. 15) for all hydraulic fracturing data. Similarly, for overcoring test data, the misfit is defined by Eq. 16.

$$\psi^{OC} = \sum_{n=1}^N \frac{|S_{mes2}^n - S_{cal2}^n|}{S_d^n} \tag{16}$$

Where S_{mes2} and S_{cal2} are the measured and calculated (simulated) stresses, respectively, S_d is the uncertainty in stress measurements (standard deviation in the present case) and N is the total number of measured stress data by the overcoring method. In Eq. 16, the uncertainty associated with the borehole direction is neglected because overcoring tests were conducted within a maximum borehole length of 8 m, which is relatively short. The measured stresses are expressed in six different components in order to consider both magnitude and orientation of the stresses. The principal stresses presented in Table 1 are therefore transformed to the global coordinate system. The statistical values of transformed stresses are presented in Table 15. The stress data are then used to calculate the overall misfit (Eq. 16) for all overcoring data of the UTHP.

Since the hydraulic fracturing and overcoring methods are of different nature and concern different rock volumes, a global misfit function for the combined data set should be defined by introducing the weighing factors (Ask 2006 and Figueiredo et al. 2014). The weighing factors take into account the volume or the area involved by the measurement for each of the methods. The general global misfit function is hence expressed by Eq. 17.

$$\psi^{HFOC} = \omega^{HF} \psi^{HF} + \omega^{OC} \psi^{OC} \tag{17}$$

Where the respective weighing factors for each test method are expressed by Eqs. 18 and 19.

$$\omega^{HF} = \frac{A^{HF} \psi^{HF}}{A^{REV} \psi_{min}^{HF}} \tag{18}$$

$$\omega^{OC} = \frac{V^{OC} \psi^{OC}}{V^{REV} \psi_{min}^{OC}} \tag{19}$$

Where ω^{HF} , A^{HF} , and A^{REV} represent the weighting factor, the measurement area, and area involved in representative elementary volume (REV) for the hydraulic fracturing data set, respectively. Corresponding notations for the overcoring data set are ω^{OC} , V^{OC} (measurement volume) and V^{REV} (REV volume). Minimized values of individual misfit functions, ψ_{min}^{HF} and ψ_{min}^{OC} , is the median of Eqs. 15 and 16, respectively for l_1 -norm (Tarantola 2005). The area involved during hydraulic fracturing measurements depends on the injected volume and is usually of the order 1 m^2 (Ask 2006). On the other hand, the volume involved in the overcoring test is equal to the average volume of the hollow rock cylinder (Ask 2006 and Figueiredo et al. 2014). The respective area and volume involved in both tests in the UTHP are within the ranges recommended by Ljunggren et al. (2003). Further, the REV for the rock mass is assumed equal to 1 m^3 volume (i.e., 1 m^2 area) as suggested by Ask (2006) and Figueiredo et al. (2014). The combined global misfit function for the minimization of the rock stress model of the UTHP is thus expressed by Eq. 20.

$$\psi^{HFOC} = \frac{A^{HF} \psi^{HF}}{A^{REV} \psi_{min}^{HF}} \psi^{HF} + \frac{V^{OC} \psi^{OC}}{V^{REV} \psi_{min}^{OC}} \psi^{OC} \tag{20}$$

The global misfits obtained from Eq. 20 are finally minimized to define the best fit rock stress model.

Parametric analysis and model optimization

The rock mass parameters, such as elastic modulus and Poisson’s ratio, are the main parameters that could potentially induce the changes in the stress field. Since, the rock mass is assumed to be homogeneous and a linearly elastic material,

Table 15 The stresses measured by 3D overcoring in the global coordinate system (the sign convention is compatible with that in FLAC^{3D} where -ve normal stress indicates compression)

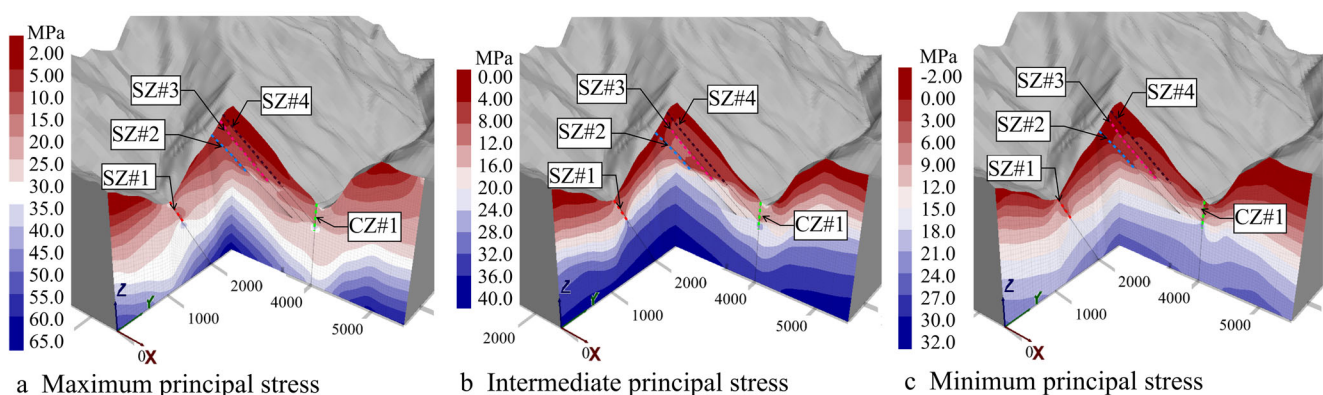
Location	S_{XX} (MPa)		S_{YY} (MPa)		S_{ZZ} (MPa)		S_{XY} (MPa)		S_{YZ} (MPa)		S_{XZ} (MPa)	
	Mean	Sd	Mean	Sd	Mean	Sd	Mean	Sd	Mean	Sd	Mean	Sd
TT1	-15.8	3.6	-10.1	2.4	-12.1	3.4	2.6	0.3	-3.7	1.0	1.7	0.88
TT2	-11.3	1.8	-11.5	2.4	-6.6	2.4	-3.2	0.0	-7.0	0.3	0.5	0.25
TT3	-12.2	3.4	-20.3	3.7	-8.2	4.3	-2.9	0.3	1.4	0.2	3.3	0.78

Table 16 Minimization of the global misfit for different combinations of tectonic stress magnitude and orientation

Trial	ν	S_{Tmax} MPa	S_{Tmin} MPa	θ Deg.	E_0^1 GPa	ψ^{HF}	ψ^{OC}	ψ^{HFOC}
1	0.25	18.0	4.0	20.0	1.2	15.9	148.1	307.2
2	0.25	18.0	4.0	25.0	1.2	16.3	115.3	287.3
3	0.25	18.0	4.0	30.0	1.2	16.4	89.6	271.9
4	0.25	18.0	6.0	20.0	1.2	13.9	180.0	336.7
5	0.25	18.0	6.0	25.0	1.2	14.4	151.8	318.1
6	0.25	18.0	6.0	30.0	1.2	14.5	130.3	289.2
7	0.25	18.0	8.0	20.0	1.2	13.2	214.3	354.8
8	0.25	18.0	8.0	25.0	1.2	13.8	191.2	336.4
9	0.25	18.0	8.0	30.0	1.2	14.0	173.5	324.7
10	0.25	20.0	4.0	20.0	1.2	16.8	124.5	306.5
11	0.25	20.0	4.0	25.0	1.2	17.2	87.2	279.6
12	0.25	20.0	4.0	30.0	1.2	17.6	87.6	293.5
13	0.25	20.0	6.0	20.0	1.2	14.4	156.4	306.1
14	0.25	20.0	6.0	25.0	1.2	14.9	123.7	287.8
15	0.25	20.0	6.0	30.0	1.2	15.0	98.8	269.5
16	0.25	20.0	8.0	20.0	1.2	13.8	190.6	338.0
17	0.25	20.0	8.0	25.0	1.2	14.4	163.0	308.7
18	0.25	20.0	8.0	30.0	1.2	14.6	141.7	282.0
19	0.25	22.0	4.0	20.0	1.2	17.7	101.0	325.0
20	0.25	22.0	4.0	25.0	1.2	18.3	90.6	326.5
21	0.25	22.0	4.0	30.0	1.2	18.7	123.3	351.7
22	0.25	22.0	6.0	20.0	1.2	14.9	132.9	288.1
23	0.25	22.0	6.0	25.0	1.2	15.4	95.7	262.9
24	0.25	22.0	6.0	30.0	1.2	15.6	83.0	265.6
25	0.25	22.0	8.0	20.0	1.2	14.4	167.0	327.2
26	0.25	22.0	8.0	25.0	1.2	15.0	134.8	294.8
27	0.25	22.0	8.0	30.0	1.2	15.1	110.1	263.5
28	0.25	20.0	5.0	25.0	1.2	15.3	105.4	259.2
29	0.25	20.0	5.0	25.0	1.0	16.0	104.5	269.7
30	0.25	20.0	5.0	25.0	1.4	14.8	106.2	252.2
31	0.25	20.0	5.0	25.0	1.6	14.3	106.8	246.8
32	0.25	20.0	5.0	25.0	1.8	14.0	107.2	242.1
33	0.25	20.0	5.0	25.0	2.0	13.7	107.6	238.4

changing the elastic modulus will not induce changes in the stress field. On the basis of the comprehensive analysis, Basnet and Panthi (2018b) concluded that the Poisson's ratio of the rock mass at the project area is at around 0.25. This value

was hence used for this study as well. It is further highlighted that both normal and shear stiffness of the interfaces depend on the value of Young's modulus (E_0) and thickness (t) of the weakness zone. In this study, t is fixed and E_0 is changed for

**Fig. 22** Magnitude of principal stresses in MPa showing stress attenuation due to the presence of deep valleys and weakness zones

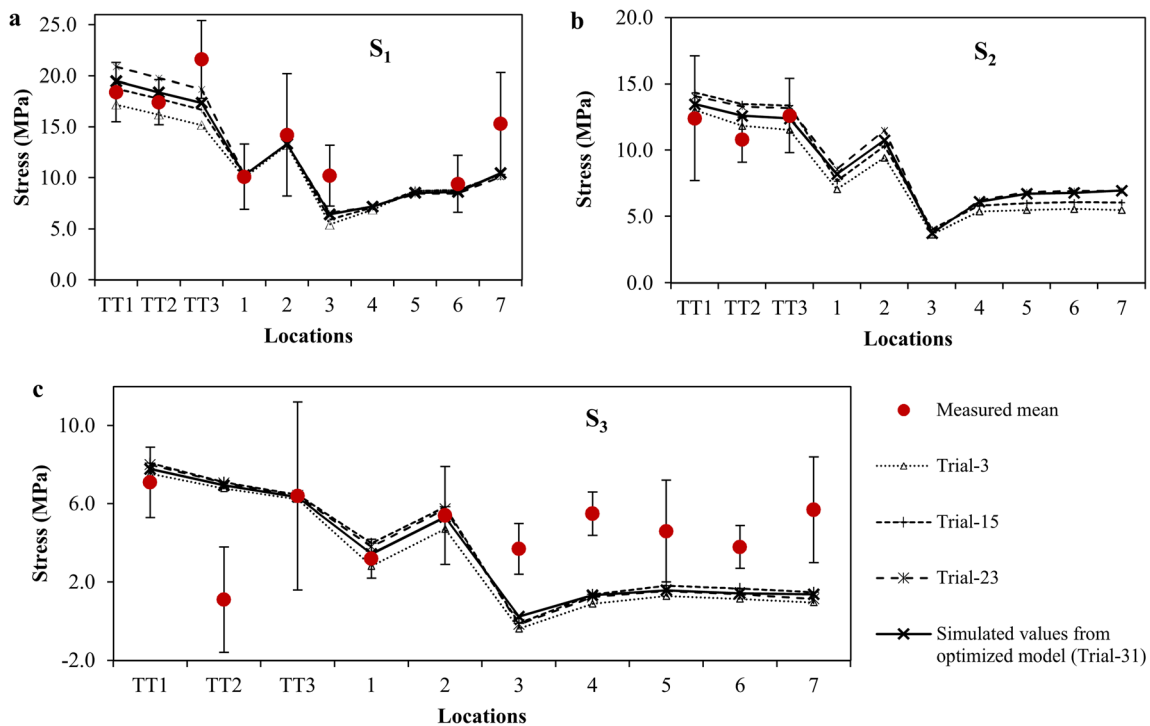


Fig. 23 The measured and simulated principal stresses; **a** maximum principal stress (S_1); **b** intermediate principal stress (S_2); **c** minimum principal stress (S_3)

the optimization process. The interface parameters presented in Table 14 for the weakness zones; CZ#1, CZ#2, CZ#3, SZ#1, and SZ#2 are used as fixed entities since these parameters were already optimized by Basnet and Panthi (2018b). The value of Young's modulus for other weakness zones, SZ#3, SZ#4, SZ#5, SZ#6, SZ#7, SZ#8, and SZ#9, is denoted by E_0^1 (Table 16) and is changed for the optimization process in the present study. First of all, both magnitude and orientation of S_{Tmax} and S_{Tmin} are changed until the global misfit is minimized for the interface parameters given in Table 15. The optimization results from trials 1 to 28 are presented in Table 16.

The influence of the 3D geometry and interfaces in the stress state and all three principal stresses are shown in Fig. 22. As one can see in the figure, the magnitudes of all three principal stresses are attenuated owing to the presence of deep valleys (i.e., both Gongar and Tamakoshi) and also the presence of weakness zones (i.e., both crushed and shear zones). It is highlighted that correct representation of 3D topographic geometry and engineering geological parameters of weakness zones are crucial in defining the best fit model.

Once the magnitude and orientation of tectonic stresses are optimized, the value of E_0^1 is changed between 1.0 GPa to

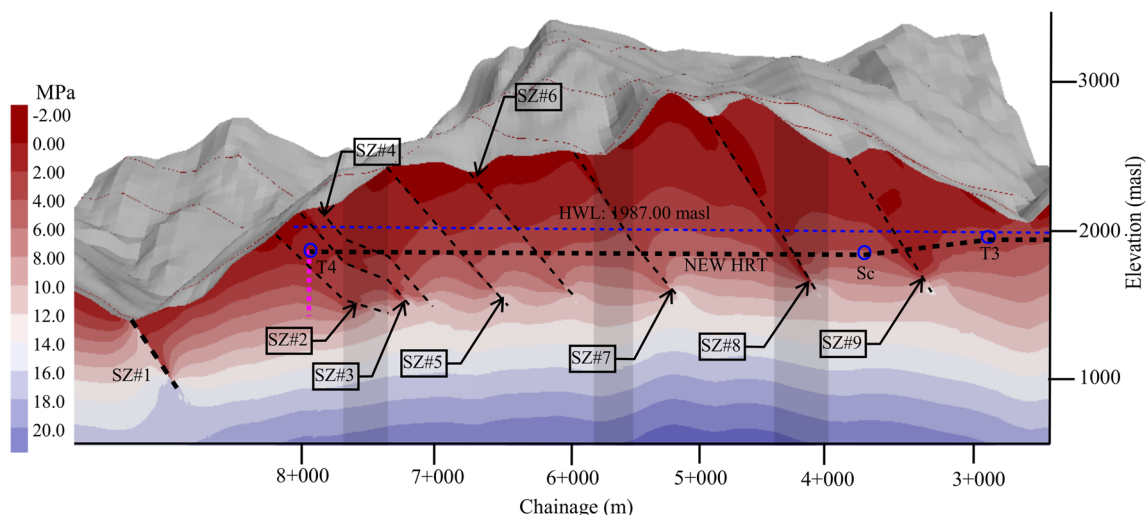
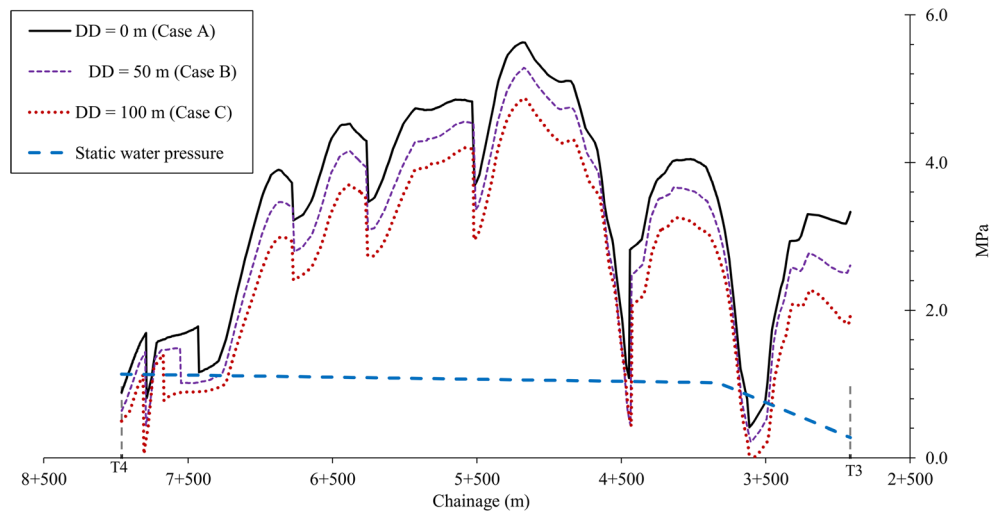


Fig. 24 Minimum principal stress along the NEW HRT (Note: color bars represent minimum principal stress in MPa)

Fig. 25 Simulated minimum principal stress along the NEW HRT at different destressed depths (DD) and static water pressure (P_w)



2.0 GPa for further optimization. It has been found that the global misfit is further reduced below the previously optimized value with the increase of E_0^1 . However, it is not logical to increase the value of E_0^1 more than 2.0 GPa as far as physical validity is concerned. The value of E_0^1 is hence fixed as 1.6 GPa to make it compatible with the value of E_0 for the rest of the weakness zones. Finally, the optimized model with the parameters as shown in trial 31 in Table 16 is considered as a best fit model for the further interpretations.

The magnitudes of the principal stresses measured at all measurement locations and corresponding simulated stresses obtained from the model at different selected trials, including the optimized trial, are further plotted in Fig. 23. The measured values are plotted with the error bars equal to one standard deviation on each side of the mean values. It has been found that the difference between measured (mean) and simulated principal stresses is less than one standard deviation for more than 55% of the test data and is less than two standard deviations for more than 80% of the test data for best fit model. The authors consider this as an acceptable condition for the model to be valid.

Analysis results

After the model is validated, the magnitude of minimum principal stresses along the headrace tunnel are extracted and shown in the tunnel profile (Fig. 24). As one can see in the figure, there is considerable stress attenuation near the shear zones along the NEW HRT.

As has been mentioned before, some locations at the surface topography inside the model extent are destressed. To account for the impact of destressed area in the stress state, the model tries to simulate this by cutting topography with the depth equal to an assumed ‘destressed depth’ (DD). More specifically, the purpose of this simulation is to quantify the impact of destressed area on the magnitude of minimum principal stress. For this, the rock mass within the destressed depth is considered as a ‘destressed rock masses’ and is assumed to have negligible contribution to the magnitude of minimum principal stress to the locations below it. The model is therefore solved for equilibrium state after the volume of rock mass equal to a uniform depth of DD is removed from the geometry shown in Fig. 18b. The model is simulated for two different

Fig. 26 Different factors of safeties along the NEW HRT

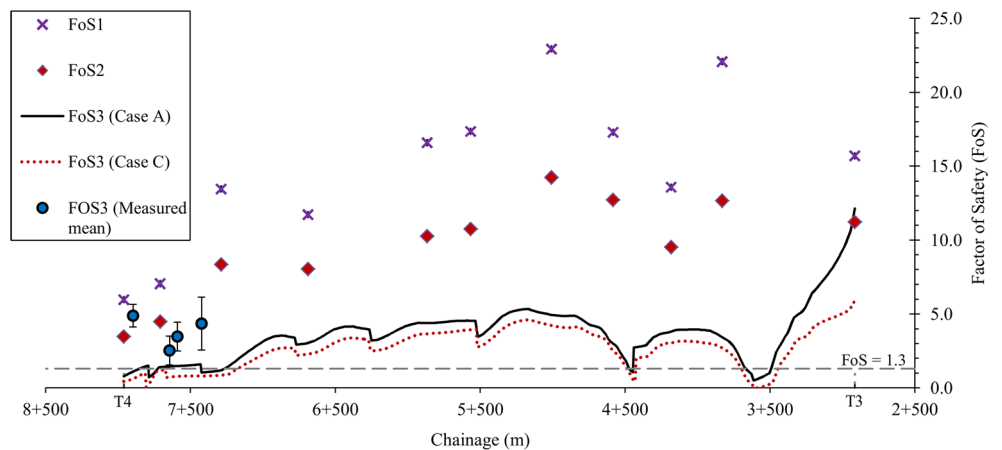


Table 17 NEW HRT alignment describing critical location against hydraulic jacking and leakage

Most critical segments	Shear zones SZ#8 and SZ#9 and the outer reach of the headrace tunnel downstream of chainage 7 + 300 m
Medium critical segments	Jointed rock mass with high hydraulic conductivity, such as joints filled with silty clay and the shear bands between chainage 2 + 914 m and 7 + 300 m.
Relatively safe segments	Most of the tunnel stretch where good to very good quality rock mass present, i.e., most of the tunnel stretch upstream of chainage 7 + 300 m excluding shear zone locations.

destressed depths, i.e., 50 m and 100 m. Hence, there are actually three different geometries altogether. First, geometry with present topography, i.e., $DD = 0$ m (Fig. 18b); second, geometry with $DD = 50$ m, and third, geometry with $DD = 100$ m. These three geometries are simulated separately as case A, case B, and case C, respectively (Fig. 25). The magnitude of minimum principal stress shown in Fig. 22 is the output of case A. The stress values along the NEW HRT are further extracted from Fig. 22 and presented in Fig. 25 as case A. Similarly, the magnitudes of minimum principal stress along the NEW HRT for case B and case C are shown in Fig. 25. The result shown in Fig. 25 suggests that the value of minimum principal stress along the headrace tunnel decreases with the increase in destressed depth. The figure also shows the static water pressure (P_w) along the NEW HRT alignment from T3 to T4. As one can see in Fig. 25, the value of minimum principal stress is less than water pressure at the tunnel locations of some weakness zones, i.e., at around chainage 3 + 600 m, at around chainage 4 + 450 m, and downstream from approximate chainage 7 + 300 m.

Findings and discussions

The qualitative assessment of the rock engineering aspects indicates that the tunnel stretches of the NEW HRT alignment where rock mass falls under the quality class of fracture rock mass (Q value between 0.1 and 4) and the rock mass of the weakness/shear zones are potentially vulnerable to hydraulic jacking and water leakage during operation. The stress state analysis carried out also supports the findings of the qualitative assessment of the rock mass. The specific findings related to the NEW HRT alignment are discussed below with the focus mainly on the critical locations of the unlined/shotcrete lined headrace tunnel.

The analysis with the Norwegian confinement criteria shows that the unlined/shotcrete lined headrace tunnel in both new and old alignments is safe against hydraulic jacking. However, both measured (absolute minimum values) and simulated minimum principal stresses at the outer reach of the old alignment are inadequate to avoid hydraulic jacking. This indicates that the ground condition at the outer reach of the headrace tunnel is not favorable to apply existing confinement criteria practiced in Norway. Along the NEW HRT alignment,

the factor of safeties given by the confinement criteria also suggests that the HRT alignment is safe against hydraulic fracturing with sufficient safety margin. On the other hand, simulated in situ stress magnitude and the rock mass quality prevailing at the downstream end of the headrace tunnel (downstream of chainage 7 + 300 m) show that this stretch of the tunnel is vulnerable against hydraulic jacking. This is mainly due to the de-stressing effect caused by multiple valley slopes toward both Gongar and Tamakoshi valleys and the presence of shear zones, which considerably reduce the magnitude of minimum principal stress. The factor of safety (FoS) beyond chainage 7 + 300 toward the downstream end is less than 1.3 indicating a high risk of hydraulic jacking at this tunnel stretch. Similarly, the corresponding factor of safety at the shear zones SZ#8 and SZ#9, i.e., approximate chainage 3 + 600 m and chainage 4 + 450 m, fall below the acceptable limit of 1.3 (Fig. 26). On the other hand, the factor of safeties at the other three shear zones (SZ#5, SZ#6, and SZ#7) are within acceptable margins.

Joints filled with silty clay and distinct local shear bands are very frequent downstream of chainage 7 + 300 m at the NEW HRT, which could function as flow paths during the operation of the project. In other locations along the tunnel alignment, the shear zones (SZ#8 and SZ#9) are also critical locations from where water may leak. The overall leakage vulnerability along the NEW HRT alignment is summarized in Table 17.

Conclusions

It is concluded that most of the NEW HRT alignment of the UTHP is safe for the implementation of the unlined/shotcrete lined high pressure tunnel excluding some critical locations where engineering geological conditions do not favor the concept. The detailed analysis carried out in assessing minimum in situ stress has also confirmed the findings of the rock engineering assessments. The most critical part of the tunnel alignment lies downstream of chainage 7 + 300 m from where there is high probability that the hydraulic jacking may occur during operation. In addition, two of the shear zones, i.e., SZ#8 and SZ#9, are also critical areas. The assessment has clearly indicated that the existing confinement criteria developed in Norway based on the rock mass and geo-tectonic conditions

prevailing in Scandinavia cannot be directly used in other geological and geo-tectonic environments. A more comprehensive approach consisting of the FRSM concept must be employed to design the unlined/shotcrete lined high pressure water tunnels. In addition, it may be useful to carry out fluid flow analysis to confirm the extent of vulnerability of the areas where hydraulic jacking is predicted to occur in this manuscript.

Acknowledgements The authors are grateful to the project management team of Upper Tamakoshi Hydroelectric Project for providing project data and information and giving permission to carry out research on this project, which will be a milestone in the use of the unlined pressure tunnel concept in the Himalayan region.

Open Access This article is distributed under the terms of the Creative Commons Attribution 4.0 International License (<http://creativecommons.org/licenses/by/4.0/>), which permits unrestricted use, distribution, and reproduction in any medium, provided you give appropriate credit to the original author(s) and the source, provide a link to the Creative Commons license, and indicate if changes were made.

References

- Ask D (2006) New developments in the integrated stress determination method and their application to rock stress data at the Äspö HRL, Sweden. *Int J Rock Mech Min Sci* 43(1):107–126
- Barton N (1973) A review of the shear strength of filled discontinuities in rock. *Fjellsprengningsteknikk, Bergmekanikk*, Oslo, Tapir Press, Trondheim, p 19.1–19.38
- Barton N (1995) The influence of joint properties in modelling jointed rock masses. 8th ISRM congress, 25–29 Sept, Tokyo
- Barton N (2002) Some new Q-value correlations to assist in site characterization and tunnel design. *Int J Rock Mech Min Sci* 39(2):185–216
- Barton N, Lien R, Lunde J (1974) Engineering classification of rock masses for the design of tunnel support. *Rock Mech* 6(4):189–236
- Basnet CB, Panthi KK (2018a) Analysis of unlined pressure shafts and tunnels of selected Norwegian hydropower projects. *J Rock Mech Geotech Eng* 10(3):1–27
- Basnet CB, Panthi KK (2018b) Evaluation on the minimum principal stress state and potential hydraulic jacking from the shotcrete lined pressure tunnel - a case from Nepal. *Rock Mech Rock Eng* 1–23. <https://doi.org/10.1007/s00603-019-1734-z>
- Benson R (1989) Design of unlined and lined pressure tunnels. *Tunn Undergr Space Technol* 4(2):155–170
- Bergh-Christensen J, Dannevig NT (1971) Engineering geological evaluations of the unlined pressure shaft at the Mauranger Hydropower Plant. Technical report. Oslo, Norway: Geoteam A/S
- Bieniawski ZT, Bernede MJ (1979) ISRM suggested methods for determining the uniaxial compressive strength and deformability of rock materials. *Int J Rock Mech Min Sci Geomech Abstr* 16(2):137–140
- Brekke TL, Ripley BD (1987) Design guidelines for pressure tunnels and shafts (No. EPRI-AP-5273). California Univ. at Berkeley, Dept. of Civil Engineering; Electric Power Research Inst., Palo Alto, CA
- Broch E (1982) The development of unlined pressure shafts and tunnels in Norway. In: *Proceedings of the ISRM International Symposium*. ISRM, p 545–54
- Broch E (1984) Unlined high pressure tunnels in areas of complex topography. *Int Water Power Dam Constr* 36(11):21–23
- Dann HE, Hartwig WP, Hunter JR (1964) Unlined tunnels of the snowy mountains hydro-electric authority. *Austr J Power Div* 90(3):47–80
- Figueiredo B, Cornet FH, Lamas L, Muralha J (2014) Determination of the stress field in a mountainous granite rock mass. *Int J Rock Mech Min Sci* 72:37–48
- Goodman RE (1989) *Introduction to rock mechanics*, vol 2. Wiley, New York, p 576
- Haimson BC, Cornet FH (2003) ISRM suggested methods for rock stress estimation—part 3: hydraulic fracturing (HF) and/or hydraulic testing of pre-existing fractures (HTPF). *Int J Rock Mech Min Sci* 40(7–8):1011–1020
- Hoek E, Diederichs M (2006) Empirical estimation of rock mass modulus. *Int J Rock Mech Min Sci* 43(2):203–215
- Holter KG, Nilsen B, Langås C, Tandberg MK (2014) Testing of sprayed waterproofing membranes for single-shell sprayed concrete tunnel linings in hard rock. In: *Proceedings of the world tunnel congress*, San Francisco
- ISRM (1978a) Suggested method for determining sound velocity. *Int J Rock Mech Min Sci Geomech Abstr. International Society for Rock Mechanics (ISRM): commission on standardization of laboratory and field tests* 15(1):55–58
- ISRM (1978b) Suggested method for determining indirect tensile strength by the Brazil test. *Int J Rock Mech Min Sci Geomech Abstr* 15(2):102–103
- ISRM (1978c) Suggested methods for the quantitative description of discontinuities in rock mass. *Int J Rock Mech Min Sci Geomech Abstr* (15):319–368
- ITASCA (2017) *FLAC3D 5.0 user's manual*. ITASCA, Minneapolis
- Li G, Mizuta Y, Ishida T, Li H, Nakama S, Sato T (2009) Stress field determination from local stress measurements by numerical modelling. *Int J Rock Mech Min Sci* 46(1):138–147
- Ljunggren C, Chang Y, Janson T, Christiansson R (2003) An overview of rock stress measurement methods. *Int J Rock Mech Min Sci* 40(7–8):975–989
- Lu M (2006) Interpretation of in-situ rock stress measurement by overcoring. *Proceedings of the international symposium on in-situ rock stress*, Trondheim, Norway, p 393–397
- MSG (2014) Hydraulic fracturing stress measurements in Upper Tamakoshi Hydroelectric Project. MeSy-Solexperts GmbH. Report no. 09.14
- MSG (2015) Hydraulic fracturing stress measurements in Upper Tamakoshi Hydroelectric Project. MeSy-Solexperts GmbH. Report no. 02.14
- Nilsen B, Palmstrom A (2000) *Engineering geology and rock engineering*. Hand book no. 2. Norwegian Group for Rock Mechanics (NBG) in co-operation with Norwegian Tunneling Society (NFF), p 1–249
- Palmstrom A, Broch E (2017) The design of unlined hydropower tunnels and shafts: 100 years of Norwegian experience. *Int J Hydropower Dams* (3):1–9
- Panthi KK (2006) Analysis of engineering geological uncertainties related to tunneling in Himalayan rock mass conditions. PhD Thesis, NTNU, Trondheim, Norway
- Panthi KK (2014) Norwegian design principle for high pressure tunnels and shafts: its applicability in the Himalaya. *Hydro Nepal: J Water, Energy Environ* (14):36–40
- Panthi KK, Basnet CB (2017) Design review of the headrace system for the upper Tamakoshi project, Nepal. *Int J Hydropower Dams* 24(1):60–67
- Parker RL, McNutt MK (1980) Statistics for the one-norm misfit measure. *J Geophys Res Solid Earth* 85(B8):4429–4430
- Rancourt AJ (2010) Guidelines for preliminary design of unlined pressure tunnels. 72(08)
- Revetz SA (2009) One-norm misfit statistics. *Geophys Res Lett* 36(20)

- Selmer-Olsen R (1969) Experience with unlined pressure shafts in Norway. Proc. Int. Symposium on large permanent underground openings, Oslo
- Selmer-Olsen R (1974) Underground openings filled with high-pressure water or air. Bull Int Assoc Eng Geol 9(1):91–95
- SINTEF (2008) Rock stress measurement at the Upper Tamakoshi hydroelectric project. SBF IN F08112
- SINTEF (2013) Rock stress measurement by hydraulic fracturing at the Upper Tamakoshi hydroelectric project, Nepal. SBF IN F08112
- Stephansson O, Zang A (2012) ISRM suggested methods for rock stress estimation—part 5: establishing a model for the in situ stress at a given site. ISRM suggested methods for rock characterization, testing and monitoring: 2007–2014, p 187–201
- Talobre, J. (1954) La mécanique des roches: appliqué aux travaux publics (In english; Rock mechanics: applied to public works). Dunod.
- Tarantola A (2005) Inverse problem theory and methods for model parameter estimation. SIAM. <https://doi.org/10.1137/1.9780898717921>
- Terzaghi K (1962) Measurement of stresses in rocks. Geotechnique 12(2):105–124
- Vogt JHL (1922) Trykktunneler og geologi (Pressure tunnels and geology). Report no. 93. Norges Geol. Undersøkelse, Oslo, Norway
- Yin JM, Cornet FH (1994) Integrated stress determination by joint inversion of hydraulic tests and focal mechanisms. Geophys Res Lett 21(24):2645–2648